NPS-OC-96-001

NAVAL POSTGRADUATE SCHOOL
MONTEREY, CALIFORNIA

THESIS

THE EFFECT OF SALINITY ON DENSITY IN THE LEEUWIN CURRENT SYSTEM

by

Ming-Jer Huang

June, 1996

Thesis Advisor: Mary L. Batteen

Approved for public release; distribution is unlimited.

Prepared for:
National Science Foundation
4201 Wilson Boulevard
Arlington, VA 22230

NAVAL POSTGRADUATE SCHOOL
MONTEREY, CALIFORNIA 93943

Rear Admiral Marsha J. Evans
Superintendent

This thesis was prepared in conjunction with research sponsored in part by the National Science Foundation, 4201 Wilson Boulevard, Arlington, VA 22230.

Released by:

G E Schacher

Gordon E. Schacher, Dean of Research (Acting)

REPORT DOCUMENTATION PAGE

Form Approved OMB No. 0704-0188

1. AGENCY USE ONLY *(Leave blank)*	2. REPORT DATE June 1996	3. REPORT TYPE AND DATES COVERED Master's Thesis

4. TITLE AND SUBTITLE THE EFFECT OF SALINITY ON DENSITY IN THE LEEUWIN CURRENT SYSTEM

5. FUNDING NUMBERS

6. AUTHOR(S) Ming-Jer Huang, in conjunction with Mary Batteen

7. PERFORMING ORGANIZATION NAME(S) AND ADDRESS(ES)
Naval Postgraduate School
Monterey, CA 93943-5000

8. PERFORMING ORGANIZATION REPORT NUMBER
NPS-OC-96-001

9. SPONSORING/MONITORING AGENCY NAME(S) AND ADDRESS(ES)
National Science Foundation
4201 Wilson Boulevard Arlington, VA. 22230

10. SPONSORING/MONITORING AGENCY REPORT NUMBER

11. SUPPLEMENTARY NOTES The views expressed in this thesis are those of the author and do not reflect the official policy or position of the Department of Defense or the U.S. Government.

12a. DISTRIBUTION/AVAILABILITY STATEMENT
Approved for public release; distribution is unlimited.

12b. DISTRIBUTION CODE

13. ABSTRACT *(maximum 200 words)*

Climatological temperature and salinity fields are used to calculate the salinity contribution to density and dynamic height fields in the Leeuwin Current System (LCS). While the temperature gradient is primarily linear, with warmest water to the north, the salinity fields are spatially inhomogenous. A comparison of density fields, calculated with constant and variable salinity, shows that, off Western Australia, the density field is primarily determined by temperature. Off Southern Australia, the density field is dependent on warm and salty (subtropical) and fresh and cold (sub-Antarctic) water masses. While the dynamic height fields, calculated with constant and variable salinity, show similar flow patterns off Western Australia, different flow patterns are found off Southern Australia.

In addition to the analysis of climatological fields, a primitive equation ocean model is used to investigate the role of salinity in the formation of currents and eddies in the LCS. Two identical ocean models, one with a climatological salinity field and the other with no horizontal salinity gradients, are run and compared with each other. Despite the model runs being initialized with similar temperature distributions, there are relatively large temperature and density differences in the Southern Australian region, due to the advection of water masses by the Leeuwin Current.

Based on the climatological analyses and the results of the model experiments, it is concluded that, descriptively and dynamically, both temperature and salinity are essential to accurately characterize the large-scale circulation of the LCS.

SUBJECT TERMS Primitive equation model, Leeuwin Current System, salinity, density, dynamic height, eddies, currents	15. NUMBER OF PAGES 76
	16. PRICE CODE

17. SECURITY CLASSIFICATION OF REPORT	18. SECURITY CLASSIFICATION OF THIS PAGE	19. SECURITY CLASSIFICATION OF ABSTRACT	20. LIMITATION OF ABSTRACT
Unclassified	Unclassified	Unclassified	UL

Approved for public release; distribution is unlimited.

THE EFFECT OF SALINITY ON DENSITY IN THE LEEUWIN CURRENT SYSTEM

Ming-Jer Huang
Lieutenant Commander, Republic of China Navy
B.S., Chung-Chang Institute of Technology - 1987

Submitted in partial fulfillment
of the requirements for the degree of

MASTER OF SCIENCE IN PHYSICAL OCEANOGRAPHY

from the

NAVAL POSTGRADUATE SCHOOL
June 1996

ABSTRACT

Climatological temperature and salinity fields are used to calculate the salinity contribution to density and dynamic height fields in the Leeuwin Current System (LCS). While the temperature gradient is primarily linear, with warmest water to the north, the salinity fields are spatially inhomogenous. A comparison of density fields, calculated with constant and variable salinity, shows that, off Western Australia, the density field is primarily determined by temperature. Off Southern Australia, the density field is dependent on warm and salty (subtropical) and fresh and cold (sub-Antarctic) water masses. While the dynamic height fields, calculated with constant and variable salinity, show similar flow patterns off Western Australia, different flow patterns are found off Southern Australia.

In addition to the analysis of climatological fields, a primitive equation ocean model is used to investigate the role of salinity in the formation of currents and eddies in the LCS. Two identical ocean models, one with a climatological salinity field and the other with no horizontal salinity gradients, are run and compared with each other. Despite the model runs being initialized with similar temperature distributions, there are relatively large temperature and density differences in the Southern Australian region, due to the advection of water masses by the Leeuwin Current.

Based on the climatological analyses and the results of the model experiments, it is concluded that, descriptively and dynamically, both temperature and salinity are essential to accurately characterize the large-scale circulation of the LCS.

TABLE OF CONTENTS

LIST OF FIGURES

LIST OF PLATES

LIST OF TABLES

ACKNOWLEDGEMENT

The author wants to thank Dr. Mary Batteen for her guidance and patience during the work in performing this investigation. A special thanks goes out to Dr. Curtis Collins for taking time to help with the dynamic height calculations. Additional thanks to Pete Braccio for his endless assistance with FERRET, UNIX, and FORTRAN programming.

I. INTRODUCTION

At a given pressure, the density of sea water depends on temperature and salinity. Except for high-latitude regions and near sources and sinks of salt, temperature is usually considered to vary more than salinity in the upper ocean and is generally considered to be the major source of density variations (Pickard and Emery, 1990).

Recent dynamic height analyses by Batteen *et al.* (1995) have shown that the distribution of salinity in the California Current System (CCS) can be important in defining the large-scale circulation of the CCS. In particular, the mean variability of salinity has been shown to be responsible for a significant equatorward component along the coast of California and a strong offshore component adjacent to Baja. Batteen *et al.* (1995) concluded that, descriptively and dynamically, both temperature and salinity are essential to accurately characterize the large-scale structure of the CCS.

Besides the CCS, other eastern boundary current (EBC) regions, such as the Leeuwin Current System (LCS), could show significant changes if salinity as well as temperature effects are considered. The Leeuwin Current is an anomalous EBC which flows poleward (against the prevailing wind direction) along the Western Australian coast, down to Cape Leeuwin (See Figure 1 for geographical locations), and swings eastward extending as far east as the Great Australian Bight (e.g., Cresswell and Golding, 1980). There is general agreement (e.g., Godfrey and Ridgway, 1985) that the Leeuwin Current is generated by a meridional pressure gradient, which overwhelms the opposing wind stress. The source for the Leeuwin Current water is predominantly geostrophic inflow from the west (e.g., McCreary *et al.*, 1986; Thompson, 1987) and is augmented by a source from the North West Shelf (e.g., Gentilli, 1972), possibly having its origin in the Pacific Ocean (Godfrey and Ridgway, 1985).

Since the Leeuwin Current is a density driven current, both temperature and salinity could contribute to its development. While the temperature gradient is primarily linear, with warmest water to the north, the salinity distribution is spatially

inhomogeneous (Figure 2). Off of Western Australia low salinity water is present to the north and northwest, high salinity to the southwest, and low salinity to the south. Depending on the time of year, these water masses could contribute to the development of the Leeuwin Current, subsurface currents, and eddies.

Here we ask the question whether salinity variability is an important consideration for defining the large-scale circulation of the LCS. To quantify the importance of salinity in the LCS, we calculate its contribution to density and to dynamic height in the LCS (Chapter II). After incorporating salinity into an ocean model (Chapter III, Section A), two identical ocean models, one with a climatological salinity field and the other with no temporal or spatial salinity gradients, are run and compared with each other (Chapter III Section B). Although the results with variable salinity included show similar features to the results with constant salinity off Western Australia, there are important quantitative differences in the Cape Leeuwin and Southern Australian regions. The low and high salinity tags in the LCS are found to be particularly useful for identifying the contributions of the different water masses to the development of the Leeuwin Current and eddies.

II. ANALYSIS OF HYDROGRAPHIC AND DYNAMIC HEIGHT FIELDS

A. ANALYSIS OF ANNUAL HYDROGRAPHIC AND DYNAMIC HEIGHT FIELDS

Two major water masses occur for all or part of the year off Western Australia (Figure 2): a warm (tropical) low salinity water mass from the North West Shelf (e.g., Weaver and Middleton, 1989) possibly having its origins in the Pacific Ocean (Godfrey and Ridgway, 1985), and a cooler (subtropical), higher saline water mass called the 'Western Australian Current' which is influenced by the presence of a large semi-permanent trough extending in a northeastward direction (Andrews, 1977).

The seas just south of Cape Leeuwin and eastward to the entrance (near Esperance in Figure 2) to the Great Australian Bight are influenced by several water types: 1) subtropical water from west of Western Australia carried in a branch of the Western Australian Current in summer (Andrews, 1977), 2) tropical water from north of Western Australia brought by the Leeuwin Current in autumn and winter (Rochford, 1969; Cresswell and Golding, 1980), and 3) local Sub-Antarctic water characterized by its coldness and low salinity (Rochford, 1986).

To explore the water masses of this area, the climatological data sets of Levitus *et al.* (1994) and Levitus and Boyer (1994) were employed. The data are gridded with one-degree horizontal resolution at standard depth levels. These data sets, which include annual and monthly mean temperature and salinity fields, were used to compute annual and seasonal density and dynamic height fields.

Before presenting the annual and monthly climatological temperature, salinity, density, and dynamic height fields, we describe how the calculations for density and dynamic height were obtained. Following Batteen *et al.* (1995), the density is computed using the following approximate equation of state for seawater:

$$\rho = \rho_0[1 - \alpha(T - T_0) + \beta(S - S_0)],$$

where α and β are the expansion and contraction coefficients for temperature T and salinity S, respectively, ρ is density, S_0 is the reference salinity, and T_0 is the reference temperature. This equation can estimate the effect of salinity for a given region if typical values of α, β, T_0, and S_0 are used. For the LCS region, α is chosen to be 2.5×10^{-4} $(^{\circ}K)^{-1}$, β is 7.5×10^{-4}, T_0 is 278.2 $^{\circ}K$ and S_0 is 35.5 psu (practical salinity units).

To assess the effect of salinity on density in the LCS, we calculate density in the above equation for variable and for constant salinity. Calculating density for variable salinity means that the density in the above equation is computed at a given level with climatological values of T and S. Calculating density for constant salinity means that the density in the above equation has S replaced by S_0, so that the above equation reduces to

$$\rho = \rho_0 [1 - \alpha(T - T_0)].$$

To assess the effect of salinity gradients on the large-scale ocean circulation of the LCS, dynamic height fields are calculated with and without the inclusion of salinity variations. The dynamic height anomaly $\Delta\Phi$ is calculated by integrating the specific volume anomaly δ over depth and comparing it with $\Delta\Phi_{35.5TP}$ (where the subscripts 35.5, T, and P stand for salinity 35.5 psu, temperature, and pressure, respectively), calculated by integrating δ_T. Comparisons between horizontal gradients of $\Delta\Phi$ and $\Delta\Phi_{35.5TP}$ are used to provide insight concerning the importance of salinity variations to the flow field. The reference level used in this study is 1000 m depth.

The climatological annual mean temperature fields are shown at 10, 100, and 200 m depth in Plate 1a, and at 400 m depth in Figure 3a. At all depths shown, the temperature distribution is primarily zonal, with the isotherms running roughly east-west. Maximum temperatures are in the north and decrease to the south. The temperature differences from north to south are ~ 11°C, 9°C, 7°C, and 2°C at 10, 100, 200, and 400 m depth, respectively.

The climatological annual mean salinity fields are shown at 10, 100, and 200 m depth in Plate 1b, and at 400 m depth in Figure 3b. The common features of the 10 and 100 m depth plots can be clearly seen: low salinity (tropical) water to the north and

northwest, high salinity (subtropical) water to the southwest, and low salinity (sub-Antarctic) water to the south. The maximum salinity for 10 m depth is centered at ~ 32°S, while the maximum salinity for 100 m depth is centered at ~ 28°S. The salinity gradient weakens from 10 to 100 m depth. The 35.5 salinity contour extends all along Southern Australia at 10 m depth, but only as far east as Albany at 100 m depth. At 200 m depth, the salinity pattern is similar to the zonal temperature pattern with maximum salinity in the north and minimum salinity in the south. At this depth, the 35.5 salinity contour extends only as far south as Fremantle (~ 32°S). At 400 m depth, the salinity difference is only 0.4 psu from north to south.

The annual density fields calculated with constant (variable) salinity at 10, 100, and 200 m depth are shown in Plate 1c (Plate 1d). The annual density fields calculated with constant (variable) salinity at 400 m depth are shown in Figure 3c (Figure 3d). A comparison of the upper levels (i.e., 10 and 100 m depth) in Plate 1c and Plate 1d shows the following. Although, off Western Australia the density is primarily determined by the temperature field, the density fields in Plate 1d are generally less dense than those in Plate 1c due to the presence of the low salinity (tropical) water mass. South of ~ 34°S, the effect of salinity on density becomes significant. In particular, off Southern Australia, the density is influenced by both the warm and salty (subtropical) water mass and the fresh and cold (sub-Antarctic) water mass. At 200 m depth, the density in Plate 1d is generally greater than that in Plate 1c due to the presence of high salinity throughout the region. At 400 m depth, the density field in both figures is relatively uniform throughout the region.

Figures 4 and 5 show the annual dynamic height patterns at 10, 100, 200, and 400 m depth for constant salinity, i.e., $\Delta\Phi_{35.5TP}$, and for variable salinity, i.e., $\Delta\Phi$, respectively. In both figures, the upper level (i.e., 10 and 100 m depth) dynamic height contours tend to be perpendicular to the west coast of Australia, which is consistent with onshore geostrophic flow toward Western Australia. Between 34°S and 36°S, while the upper level dynamic height fields in Figure 4 tend to be zonally distributed, those in Figure 5 tend to vary in both the meridional and zonal directions, due to the influence of

the salty (subtropical) water mass offshore. The lower level (i.e., 200 and 400 m depth) dynamic height patterns in both figures show equatorward flow off Western Australia, which is consistent with the depths at which the equatorward undercurrent has been observed (e.g., Thompson, 1984).

B. ANALYSIS OF SEASONAL HYDROGRAPHIC AND DYNAMIC HEIGHT FIELDS

Since the LCS has a strong seasonal (e.g., the Leeuwin Current is strongest from March to August) as well as annual cycle, the monthly mean temperature and salinity climatological fields are examined to evaluate the effects of the seasonal evolution of salinity on the density and dynamic height fields. The annual mean temperature and salinity fields showed that the water mass characteristics of the LCS are very similar at 10 and 100 m depth. Since the seasonal cycle has essentially the same vertical pattern in the upper layers, we present only the 10 m depth seasonal fields here.

The same three water masses described earlier are discussed here to help identify how salinity seasonally influences the density and dynamic height fields. These water masses are: the warm and fresh tropical water mass off northwestern Australia, the warm and salty subtropical water mass off southwestern Australia, and the cold and fresh water mass off Southern Australia.

Plate 2a shows the monthly mean temperature fields in February, May, August, and November. As the November and February plots show, the temperature gradient off Western Australia during the austral spring and summer has a 45 degree slope from northeast to southwest, which provides the source for an onshore geostrophic current (i.e., the Leeuwin Current). As the May and August plots show, the slope becomes even steeper during the austral fall and winter, which is consistent with the Leeuwin Current being strongest during this period. Off Southern Australia, except for the advection of the Leeuwin Current in the vicinity of Cape Leeuwin during the austral fall and winter, the

temperature pattern follows a typical seasonal cycle of warmest (coldest) temperature off the coast in summer (winter).

Plate 2b shows the monthly mean salinity fields in February, May, August, and November. In February, the salinity field shows a zonal distribution of fresh water in the north, which becomes saltier poleward to ~ 32°S. There is an offshore region of maximum salinity of ~ 35.8 from ~ 28°S to 35°S, centered at ~ 32°S. South of ~ 35°S, fresher water is found. In May, the salinity gradient has a 45 degree slope off Western Australia. The maximum salinity has shifted southward to ~ 34°S. In August, the fresh water off northwest Australia has moved farther southward, while the maximum salinity has moved farther offshore. In November, off northwest Australia, the fresh water has been replaced by more saline water. The maximum salinity has retreated equatorward to ~ 31°S.

The density fields shown in Figures 6a and 6b were calculated with constant and variable salinity, respectively. In general, throughout the year, the density fields off Western and Southern Australia in Figure 6b are less dense than those in Figure 6a, due to the presence of low salinity (tropical and sub-Antarctic) water masses. In the southwestern Australia region, the density fields in Figure 6b are more dense than those in Figure 6a because of the presence of the salty (sub-tropical) water mass.

Figures 7a and 7b show the seasonal dynamic height patterns for constant and variable salinity, respectively. In both figures, throughout the year, off Western Australia, the dynamic height flow pattern is consistent with onshore geostrophic flow toward Western Australia. In contrast, south of 36°S, while the dynamic height fields in Figure 7a tend to be zonally distributed throughout the year, those in Figure 7b tend to be vary in both the meridional and zonal directions, due to the influence of the salty (subtropical) water mass offshore.

To quantify the seasonal effect of salinity on the dynamic height field, the dynamic height field at several offshore and nearshore locations were calculated. Figure 8 shows the meridionally averaged dynamic height field at 108.5°E from 1) 22°S to 29°S,

2) 30°S to 35°S, and 3) 36°S to 40°S. In region 1, the dynamic height with variable salinity (solid line) is similar to that with constant salinity (dashed line). In the other two regions, the dynamic height fields are dependent on both temperature and salinity from ~ May to August in region 2 and for most of the year in region 3. In region 2, the seasonal dependence on both temperature and salinity coincides with the time frame that the Leeuwin Current is strongest. In region 3, the seasonal salinity effect is consistent with the time that the subtropical salty water moves poleward to ~ 40°S.

The dynamic height fields calculated at several nearshore locations are shown in Figure 9. In the nearshore regions 1 and 2, which correspond to coastal locations off Western Australia, because the salinity gradient is not as strong as in the offshore regions, the salinity effect is not very significant in these regions. In contrast, in the nearshore region 3, which corresponds to a coastal location off Southern Australia, the dynamic height is dependent on both temperature and salinity throughout most of the year, indicating that in this region salinity plays a very important role.

III. EFFECT OF SALINITY ON AN OCEAN MODEL OF THE LCS

A. THE MODEL

1. Model Description

The numerical model in this study was originally used for a coarse resolution, closed basin by Haney (1974), and later adapted for eddy-resolving, limited EBC regions with open borders on the northern, western, eastern, and southern boundaries by Batteen *et al.* (1989, 1996) and Batteen (1996). The limited area EBC model is multi-level, uses non-adiabatic primitive equations on a beta-plane, and has both baroclinic and barotropic velocity components. The model is based on the hydrostatic, Boussinesq, and rigid lid approximations. The governing equations are as follows:

$$\frac{du}{dt} = \frac{-1}{\rho_0}\frac{\partial p}{\partial x} + fv - A_M \nabla^4 u + K_M \frac{\partial^2 u}{\partial z^2} \tag{1}$$

$$\frac{dv}{dt} = \frac{-1}{\rho_0}\frac{\partial p}{\partial y} - fu - A_M \nabla^4 v + K_M \frac{\partial^2 v}{\partial z^2} \tag{2}$$

$$\frac{\partial u}{\partial x} + \frac{\partial v}{\partial y} + \frac{\partial w}{\partial z} = 0 \tag{3}$$

$$\frac{\partial p}{\partial z} = -\rho g \tag{4}$$

$$\rho = \rho_0[1 - \alpha(T - T_0) + \beta(S - S_0)] \tag{5}$$

$$\frac{dT}{dt} = -A_H \nabla^4 T + K_H \frac{\partial^2 T}{\partial z^2} \tag{6}$$

$$\frac{dS}{dt} = -A_H \nabla^4 S + K_H \frac{\partial^2 S}{\partial z^2} \quad . \tag{7}$$

In the above equations, t is time, (x,y,z) is a right-handed Cartesian coordinate system with x pointing toward shore, y alongshore, and z upward. The corresponding velocity components are (u,v,w), T is temperature, S is salinity, ρ is density, and p is

pressure. Table 1 provides a list of other symbols found in the model equations, as well as values of constants used throughout the study.

For the finite differencing, a space-staggered B-scheme (Arakawa and Lamb, 1977) is used in the horizontal. Batteen and Han (1981) have shown that this scheme is appropriate when the grid spacing is approximately on the same order as, or less than, the Rossby radius of deformation, which meets the criteria of this study. The horizontal grid spacing is 14 km in the north-south direction and 11 km in the east-west direction, while the internal Rossby radius of deformation is ~ 30 km. In the vertical, the 10 layers are separated by constant z-levels of 13, 46, 98, 182, 316, 529, 870, 1416, 2283, and 3656 m. This spacing scheme concentrates more on the upper, dynamically active part of the ocean, above the thermocline.

The model domain (Figure 2) is a rectangular region encompassing the west and south coasts of Australia, from ~ 22.5°S to 40°S (1792 km alongshore), and from ~107.5°E to 122.5°E (1408 km cross-shore). The coastal boundaries of the model domain are closed, and have both the tangential and normal components of velocity set to zero. Bottom topography has been omitted to focus on the roles played by thermal and saline forcing. The constant depth used in the model is 4500 m. A modified version of the radiation boundary conditions of Camerlengo and O'Brien (1980) is used for the open ocean domain boundaries to the north, south, east and west. Some spatial smoothing is applied in the vicinity of the open boundaries.

The model uses biharmonic lateral heat and momentum diffusion with the same choice of coefficients (i.e., $2.0 \times 10^{17} cm^4 s^{-1}$) as in Batteen *et al.* (1989). Holland (1978) showed that the highly scale-selective biharmonic diffusion acts predominantly on submesoscales, while Holland and Batteen (1986) found that baroclinic mesoscale processes can be damped by Laplacian lateral heat diffusion. As a result, the use of biharmonic lateral diffusion should allow mesoscale eddy generation via barotropic (horizontal shear) and/or baroclinic (vertical shear) instability mechanisms. As in Batteen *et al.* (1989), weak ($0.5 cm^2 s^{-1}$) vertical eddy viscosities and conductivities are used.

Bottom stress is parameterized by a simplified quadratic drag law (Weatherly, 1972), as in Batteen *et al.* (1989).

2. Method of Solution

Equations (1) through (7) comprise a closed system of seven scalar equations and seven unknowns, u, v, w, p, ρ, T, and S. The variables, u, v, T, and S are prognostic variables whose time rates of change are predicted from (1), (3), (6) and (7), respectively. Although the diagnostic variables w, p, and ρ can be determined from (3), (4), and (5), respectively, there are additional constraints imposed on p and w by the choice of the rigid lid boundary conditions. The vertically integrated pressure can no longer be obtained by integrating the hydrostatic equation (4) for the free surface. Further, the vertically-integrated horizontal velocity is constrained to be non-divergent, i.e.,

$$\int_H^0 \left(\frac{\partial u}{\partial x} + \frac{\partial v}{\partial y} \right) d\varepsilon = 0 \ , \tag{8}$$

which is obtained by integrating (3) and applying the vertical boundary conditions.

For any quantity q, let its vertical average be denoted by $\bar{q}$ and its departure (vertical shear) by q'. From (8) the vertical mean flow can then be described by a streamfunction ψ, such that:

$$\bar{u} = \frac{1}{H} \frac{\partial \psi}{\partial y} \quad , \tag{9}$$

$$\bar{v} = \frac{1}{H} \frac{\partial \psi}{\partial x} \quad . \tag{10}$$

The streamfunction ψ is predicted from the vorticity equation, which is derived from the vertical average of (1) and (2). Applying the curl operator to the vertical average (1) and (2), and using (9) and (10), the vorticity equation is

$$\frac{\partial \zeta}{\partial t} = \frac{\partial}{\partial t}\left[\frac{1}{H}\left(\frac{\partial^2 \psi}{\partial x^2}\right) + \frac{1}{H}\left(\frac{\partial^2 \psi}{\partial y^2}\right) + \frac{\partial \psi}{\partial x}\frac{\partial H^{-1}}{\partial x} + \frac{\partial \psi}{\partial y}\frac{\partial H^{-1}}{\partial y}\right]$$
$$= -\left[\frac{\partial}{\partial x}\left(\frac{f}{H}\frac{\partial \psi}{\partial y}\right) - \frac{\partial}{\partial y}\left(\frac{f}{H}\frac{\partial \psi}{\partial x}\right)\right]$$
$$-\left[\frac{\partial}{\partial x}\left(\frac{g}{H\rho_0}\int_H^0\int_z^0 \frac{\partial \rho}{\partial y}\,d\varepsilon dz\right) - \frac{\partial}{\partial y}\left(\frac{g}{H\rho_0}\int_H^0\int_z^0 \frac{\partial \rho}{\partial x}\,d\varepsilon dz\right)\right] \quad (11)$$
$$+\frac{\partial}{\partial x}\left(\frac{1}{H}\int_H^0 G dz\right) - \frac{\partial}{\partial y}\left(\frac{1}{H}\int_H^0 F dz\right),$$

where G and F represent the collected contributions of the nonlinear and viscous terms in equations (1) and (2).

The vorticity equation (11) is solved by obtaining an updated value of ζ by application of the leapfrog (or every 11 time steps, the Euler-backward) time-differencing scheme. The associated value of ψ can then be obtained from:

$$\zeta = \frac{1}{H}\left(\frac{\partial^2 \varphi}{\partial x^2}\right) + \frac{1}{H}\left(\frac{\partial^2 \varphi}{\partial y^2}\right) + \frac{\partial \psi}{\partial x}\frac{\partial H^{-1}}{\partial x} + \frac{\partial \psi}{\partial y}\frac{\partial H^{-1}}{\partial y}, \quad (12)$$

which is an elliptic equation. A solution to (12) is fully prescribed by specifying the values of ψ on the open and closed boundaries of the model domain. Currently, to solve (12), the model uses an elliptic solver when there are no variations in coastline geometry and/or topography, and successive over-relaxation techniques when there are variations in coastline geometry and/or topography.

The vertical shear current (u', v') is predicted from (1) and (2) after subtracting the vertical mean. The results are:

$$\frac{du'}{dt} = \frac{-1}{\rho_0}\frac{\partial p'}{\partial x} + fv' - A_M \nabla^4 u' + K_M \frac{\partial^2 u'}{\partial z^2} + F - \overline{F} - \frac{\tau^y}{\rho_0 H}, \quad (13)$$

$$\frac{dv'}{dt} = \frac{-1}{\rho_0}\frac{\partial p'}{\partial y} - fu' - A_M \nabla^4 v' + K_M \frac{\partial^2 v'}{\partial z^2} + G - \overline{G} - \frac{\tau^x}{\rho_0 H}. \quad (14)$$

In (13) and (14), p', which represents the departure of the pressure from the vertical average, is , using (4), expressed in terms of ρ as:

$$\rho' = \int_z^0 \rho g d\varepsilon - \frac{1}{H}\int_H^0 \left(\rho g d\varepsilon\right) dz \quad , \tag{15}$$

where ε is a dummy variable representing the vertical coordinate.

The method of solution consists of predicting $\nabla^2\psi, \psi, u', v', T,$ and S from (11), (12), (13), (14), (6) and (7), respectively. The total current is then obtained by adding the vertical shear part to the vertical average part, after the latter is obtained from ψ using (9) and (10). The diagnostics ρ, w, and p' are obtained from (5), (8), and (15), respectively.

3. Forcing Conditions and Experimental Design

Previous experiments by Batteen and Rutherford (1990) and Batteen *et al.* (1992) investigated the role of thermal forcing in generating the Leeuwin Current and eddies off Western Australia with a model domain which was a closed eastern boundary with open borders to the north, south, and west. The model was initialized with climatological thermal forcing from Levitus (1982), and the ocean was then allowed to geostrophically adjust in the absence of external forcing.

In a more recent study by Batteen *et al.* (1996), thermal forcing conditions from Levitus et al. (1994) and Levitus and Boyer (1994) were used. In addition, the forcing was continuously applied at the western boundary, and the model domain was expanded to include the Southern Australian region, an area rich with observations of currents and eddies, but lacking in eddy-resolving modeling studies of the region. Model developments included the opening up of the eastern boundary in the vicinity of Esperance in Southern Australia, and the incorporation of an irregular coastline into the model.

In this study, to explore the additional effect of salinity on the LCS, both annual and seasonal salinity forcing conditions from Levitus *et al.* (1994) and Levitus and Boyer (1994) have been incorporated into the model. The annual (seasonal) temperature and salinity forcing conditions for the upper five levels (top level), which are assumed to be

zonally homogenous, are shown in Figure 10 (Figure 11). For both annual and seasonal forcing conditions, since the lower five levels do not exhibit much horizontal variation, they are assumed to be constant for each level. The temperature values used for levels 6 to 10 are 9.53°C, 6.03°C, 3.24°C, 2.19°C, and 1.27°C. The salinity constant used for the lower five levels is 34.7.

The solid, dashed, and dotted lines plotted in Figure 11 correspond to latitudinal regions where the three water masses discussed earlier are found. Regardless of the region, the temperature conditions (Figure 11a) indicate that there is, as expected, a temperature maximum in March (austral summer) and a temperature minimum in September (austral winter) throughout the whole region. The salinity conditions (Figure 11b) show relatively strong aperiodic (non-seasonal) variations throughout the year for all of the regions presented.

The design of the model experiments (see Table 2) is as follows. Experiments 1 and 2 study the model response to annual forcing. Experiment 1 uses the variable thermal and salinity forcing conditions shown in Figures 10a and 10b. Experiment 2 uses the same variable thermal forcing conditions but has salinity set to a constant such that S is replaced by S_0 in equation (5). Experiments 3 and 4 study the model response to seasonal forcing. Experiment 3 uses the variable thermal and salinity forcing conditions shown in Figures 11a and 11b. Experiment 4 uses the same variable thermal forcing conditions but has salinity set to a constant such that S is replaced by S_0 in equation (5).

B. RESULTS FROM MODEL SIMULATIONS

In each of the experiments, the model integrations start from a state of rest. Once a day, the model is updated at the western boundary with annual or seasonal forcing conditions. To ensure that the time period when the Leeuwin Current is strongest (~ April to September), is incorporated in the model, each model integration is run for a full year.

Although we are interested in the difference between model runs with variable salinity and with constant salinity, we first show that the model produces reasonable

results. The main phenomena in the LCS is the density-driven Leeuwin Current, which flows poleward off Western Australia and eastward off Southern Australia; an equatorward undercurrent found below the Leeuwin Current off Western Australia; and eddies. Figures 12 and 13 show that the Leeuwin Current with velocities of ~ 30-100 cm/s, an equatorward undercurrent with core velocities of ~ 5-15 cm/s, and anticyclonic eddies (one just south of Shark Bay, one between Dongara and Fremantle, and one in the vicinity of Cape Leeuwin) are reproduced in the model. The results from model runs are qualitatively similar and compare well with available observations of the LCS (e.g., Boland *et al.*, 1988; Cresswell and Golding, 1980).

1. Experiments 1 and 2 - Annual Thermal and Salinity Forcing Experiments

The annual forcing model integration with variable salinity (Experiment 1) and that with constant salinity (Experiment 2) begin with identical temperature distributions. When the two integrations are compared with each other, significant differences are found, as is illustrated here for the time period that the Leeuwin Current is strongest (~ April to September, corresponding to model days 90 to 273). Differences of up to 4°C are noted during this time period (Figure 14a), due to the advection of warmer (21°C or greater) water in Experiment 1 by the Leeuwin Current between Cliffy Head and Albany (compare Figure 15a with 15b). Farther east, between Albany and Esperance, the temperature difference of ~ 3°C in Experiment 1 is due to the trapping of warmer water nearshore by the Leeuwin Current.

The time-averaged salinity field (Figure 16) shows that the three major water masses discussed earlier (see Figure 2) are reproduced well in the LCS model, i.e., fresh (<35.5) water is found off the northern part of Western Australia, salty (>35.5) water offshore of Western Australia and Cape Leeuwin, and fresh (<35.5) water to the south.

The time-averaged density fields (Figures 17a and 17b), along with the density difference between Experiments 1 and 2 (Figure 14b) show the following. The density differences north of 34°S are relatively small. The water for Experiment 1 off the

northern part of Western Australia is less dense than that in Experiment 2, due to the combination of warm and fresh water in the region, while offshore of Western Australia, the water for Experiment 1 is more dense, due to the combination of salty and warm water.

The largest density differences (Figure 14b) are found between Cape Leeuwin and Esperance. The water off Cape Leeuwin in Experiment 1 is more dense than that in Experiment 2 due to the saltier water. The water between Cliffy Head and Albany is less dense in Experiment 1 than in Experiment 2, due to the much warmer (up to 4°C) water in the region. The water east of Albany is more dense in Experiment 1 than in Experiment 2, due to the saltier water nearshore which has been advected into the region by the Leeuwin Current.

2. Experiments 3 and 4 - Seasonal Thermal and Salinity Forcing Experiments

Since the LCS has significant temporal variability in salinity (see Figure 11b), Experiments 3 and 4 are designed to study the model response to seasonal forcing, both using the same thermal forcing conditions but with variable (Experiment 3) and constant (Experiment 4) salinity. As in the previous experiments, here we focus on the difference between the two model runs to identify the salinity effect on density. During the time period that the Leeuwin Current is strongest, differences of up to 2°C are noted (Figure 18a) due to the displacement of warm, anticyclonic eddies by the Leeuwin Current in the Southern Australian region.

North of 34°S, the density differences (Figure 18b) show that the water for Experiment 3, compared to Experiment 4, is less dense off Western Australia and more dense offshore of Western Australia. The water off Cape Leeuwin in Experiment 3 is more dense than that in Experiment 4 due to the combination of salty and warm water in the region. The water between Cliffy Head and Albany is less dense, due to the displacement of warm (up to 2°C), anticyclonic eddies by the Leeuwin Current in the region.

IV. SUMMARY

This study used climatological temperature and salinity fields to calculate the salinity contribution to density and dynamic height fields in the Leeuwin Current System (LCS). While the temperature gradient is primarily linear, with warmest water to the north, the salinity field is spatially inhomogeneous with low salinity (tropical) water to the north and northwest, high salinity (subtropical) water to the southwest, and low salinity (sub-Antarctic) water to the south. A comparison of annual density fields, calculated with constant and variable salinity, showed that, off Western Australia, the density field was primarily determined by temperature. South of 34°S, the effect of salinity on density became significant. In particular, off Southern Australia, the density was shown to be influenced by both the warm and salty (subtropical) water mass and the fresh and cold (sub-Antarctic) water mass. The seasonal density field patterns were found to be similar to the annual density field patterns.

The annual dynamic height fields, calculated with constant and variable salinity, showed similar flow patterns off Western Australia but different flow patterns between 34°S and 36°S. Throughout the year, the seasonal dynamic height fields calculated with constant and variable salinity showed similar flow patterns off Western Australia and different flow patterns south of 36°S.

In addition to the analysis of the climatological temperature and salinity fields, a high resolution, multi-level, primitive equation model was used to investigate the role of salinity in the formation of currents and eddies in the LCS. After incorporating salinity into the model, two identical ocean models, one with a climatological salinity field and the other with no horizontal salinity gradients, were run and compared with each other.

Experiments 1 and 2 used annual thermal and salinity conditions to initialize and force the model. Despite the model runs being initialized with the same temperature distributions, differences of up to 4°C were noted during the time period that the Leeuwin Current was strongest in the Southern Australian region, due to the advection of warmer

water by the Leeuwin Current between Cliffy Head and Albany. Large density differences were also found between Cape Leeuwin and Esperance, where the salinity effect on density became significant.

Experiments 3 and 4 used seasonal thermal and salinity conditions to initialize and force the model. During the time period that the Leeuwin Current was strongest, differences of up to 2°C were noted in the Southern Australian region, due to the displacement of warm, anticyclonic eddies by the Leeuwin Current nearshore. Large density differences were also found between Cape Leeuwin and Albany, where the salinity effect on density became significant.

The results from both the climatological analysis and the model experiments strongly suggest that there are important quantitative differences between constant and variable salinity calculations, particularly in the Cape Leeuwin and Southern Australian regions. The low and high salinity tags in the LCS are found to be particularly useful for identifying the contributions of the different water masses to the development of the Leeuwin Current and eddies.

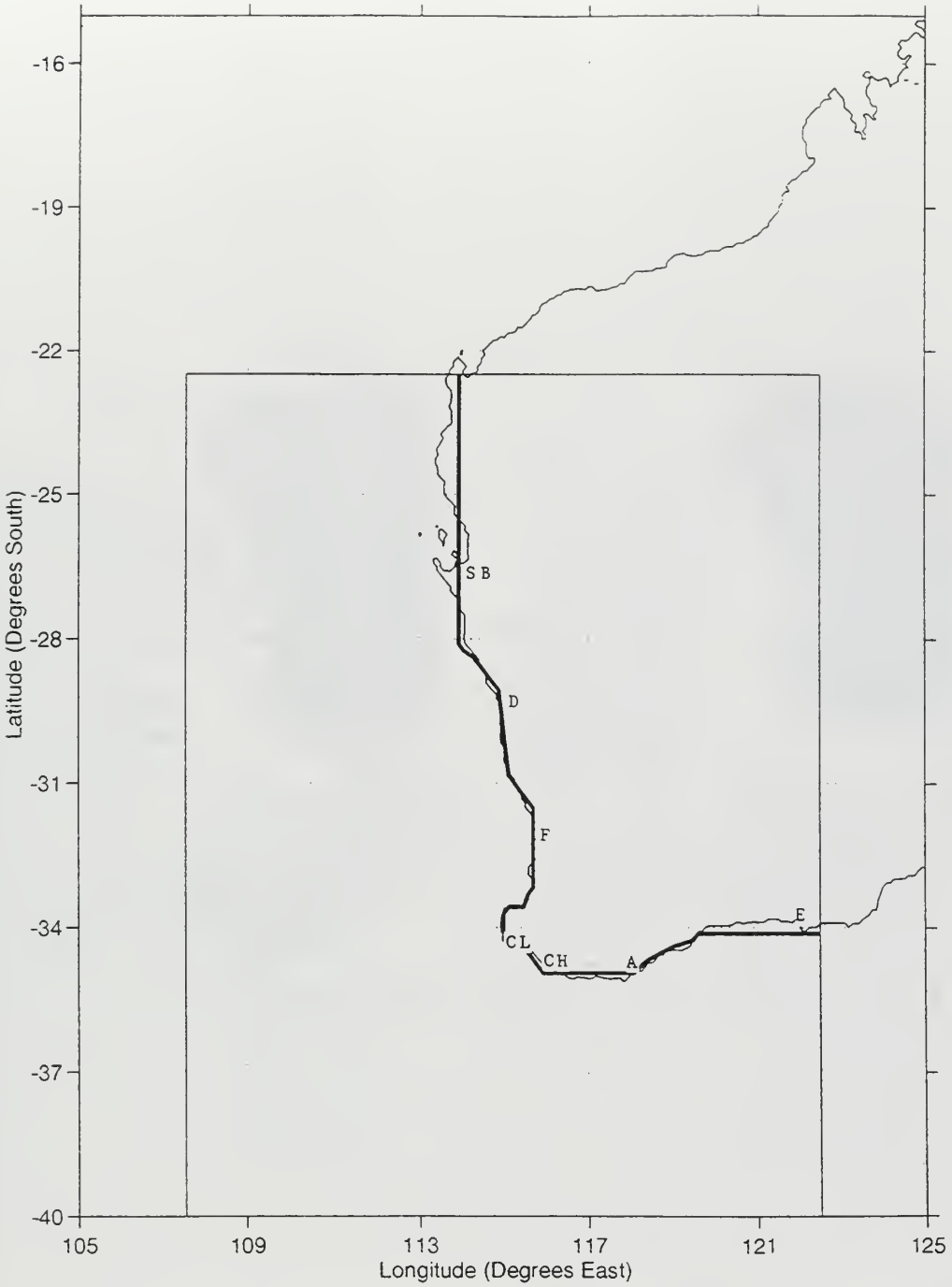

Figure 1. Box shows the domain of the model for the Leeuwin Current System (LCS) off Western and Southern Australia. Domain is bounded by 22.5°S to 40°S, 107.5°E to 122.5°E. The irregular coastline (solid line) used in the model includes Shark Bay (SB), Dongara (D), Fremantle (F), Cape Leeuwin (CL), Cliffy Head (CH), Albany (A), and Esperance (E).

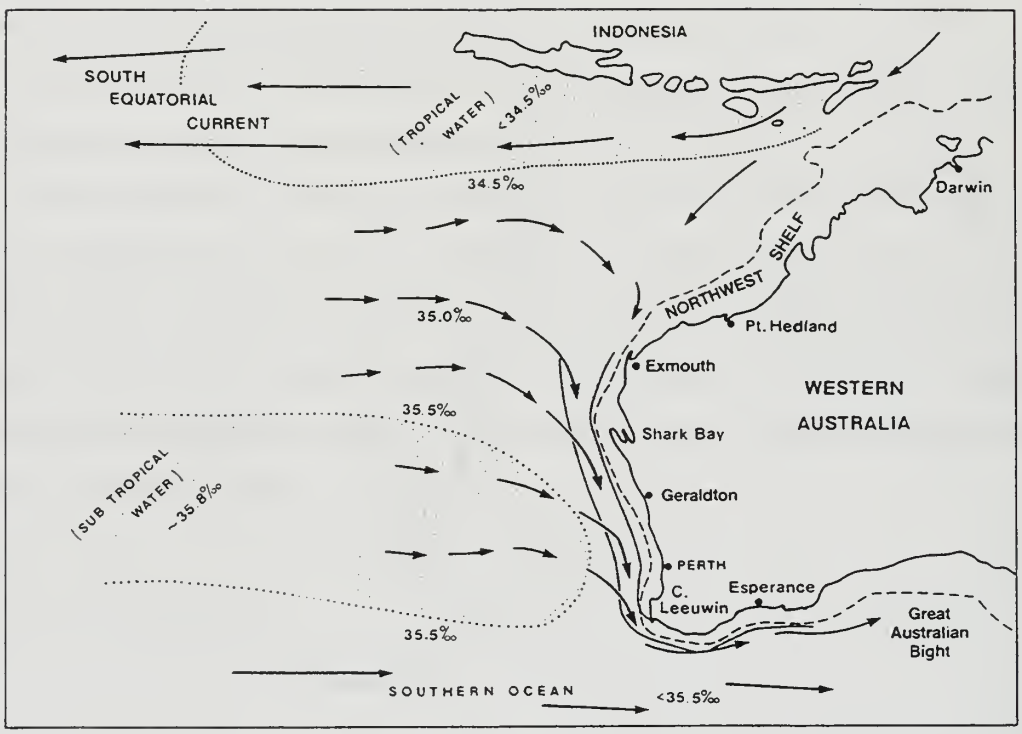

Figure 2. Schematic chart of the mean large-scale circulation in the eastern Indian Ocean. The tropical (salinity < 34.5) and subtropical (> 35.8) water masses are shaded. The edge of the continental shelf (200 m isobath) is dashed. The Leeuwin Current is the southward flow of warm low-salinity water down the Western Australian coast. (from Pearce and Cresswell, 1985)

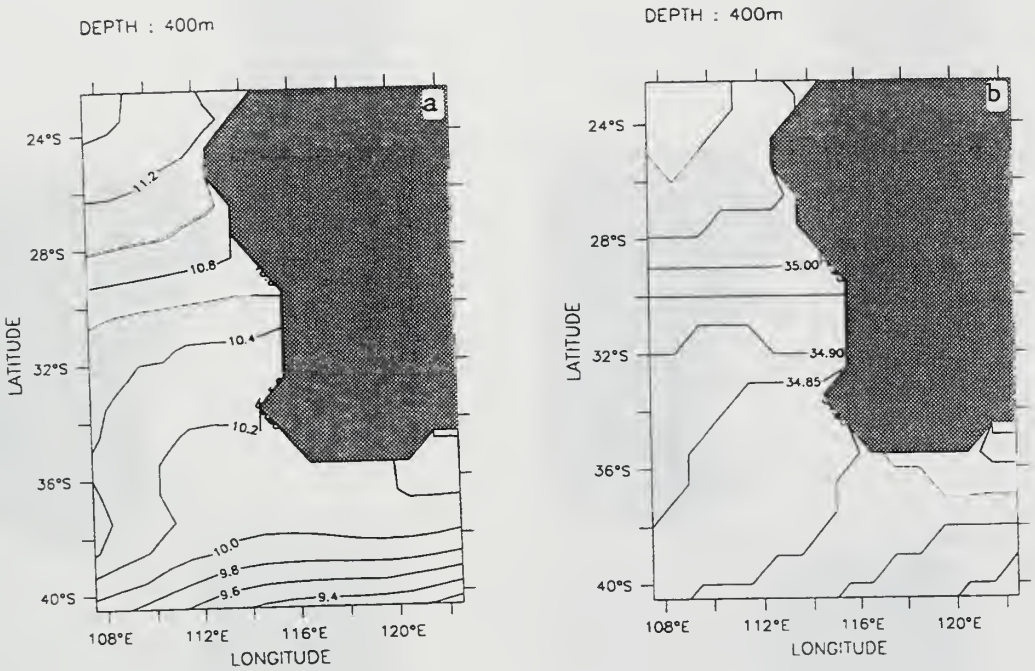

Figure 3. Annual temperature (a) and salinity (b) fields at 400 m depth. Annual density field with constant (c) and variable (d) salinity at 400 m depth. The contour interval is 0.2°C in (a), 0.05 psu in (b) and 0.05 in (c) and (d).

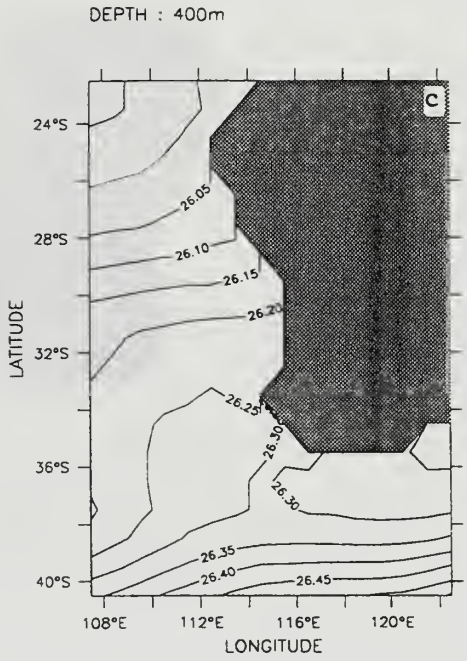
DEPTH : 400m
c
24°S
28°S
32°S
36°S
40°S
LATITUDE
26.05
26.10
26.15
26.20
26.25
26.30
26.35
26.40
26.45
108°E
112°E
116°E
120°E
LONGITUDE

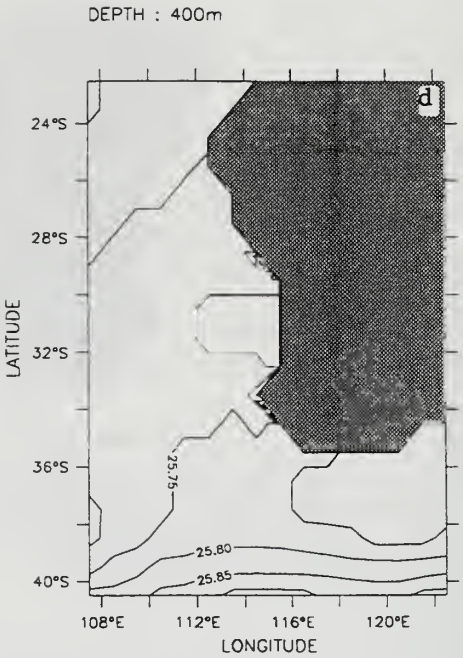
DEPTH : 400m
d
24°S
28°S
32°S
36°S
40°S
LATITUDE
25.75
25.80
25.85
108°E
112°E
116°E
120°E
LONGITUDE

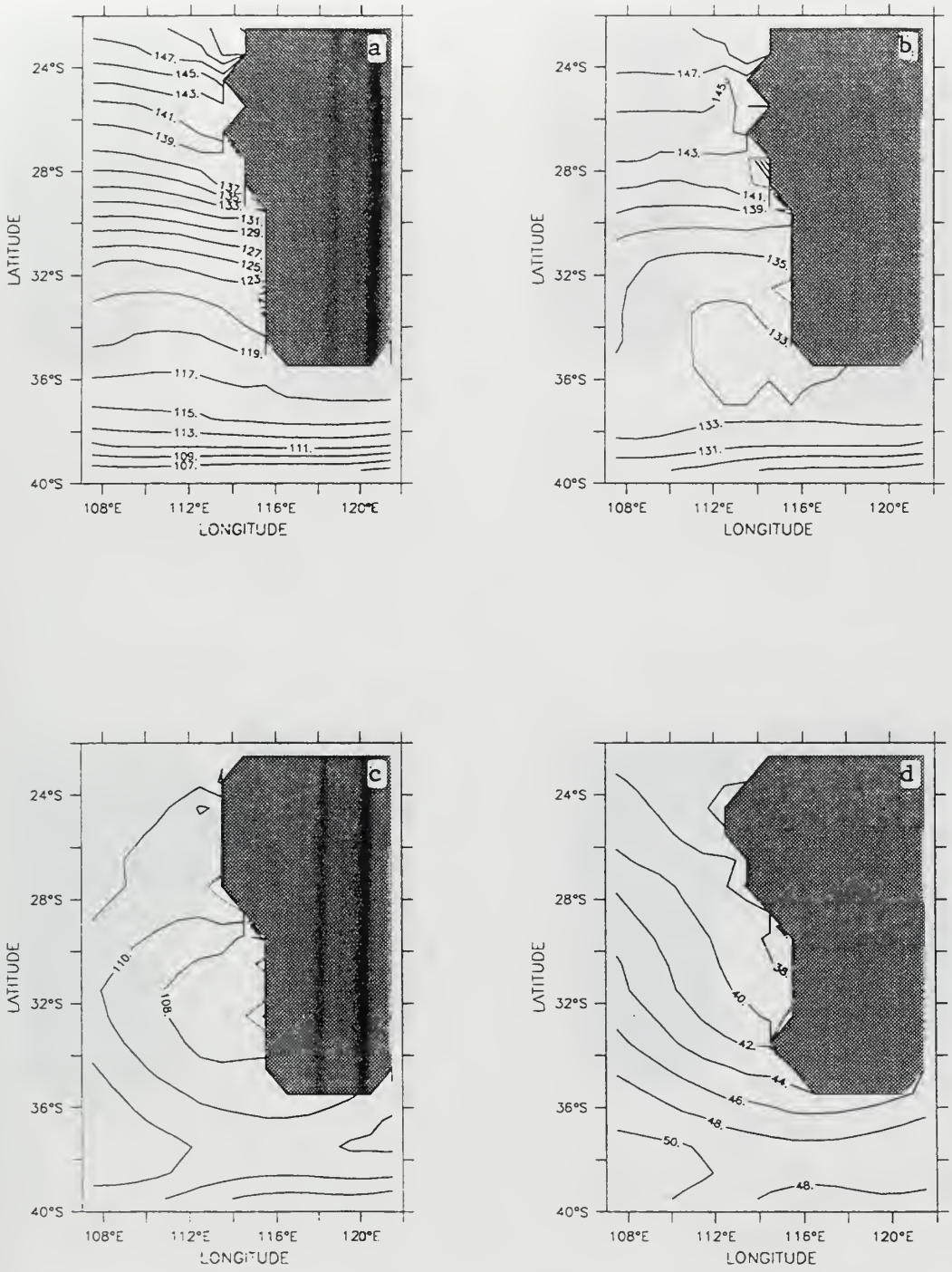

Figure 4. Annual dynamic height field with constant salinity at (a) 10, (b) 100, (c) 200, and (b) 400 m depth. The contour interval is 2 dyn. cm.

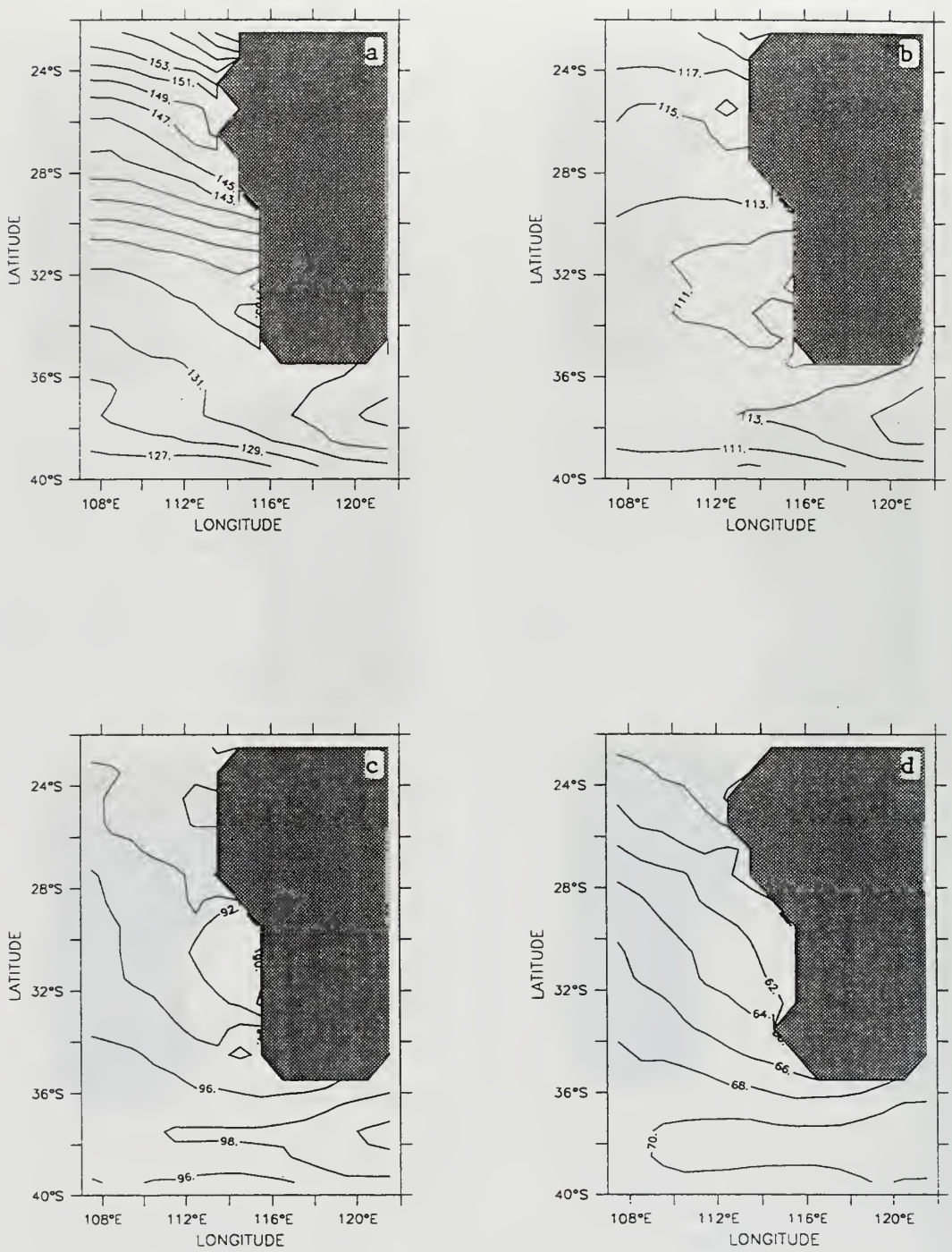

Figure 5. Annual dynamic height field with variable salinity at (a) 10, (b) 100, (c) 200, and (d) 400 m depth. The contour interval is 2 dyn. cm.

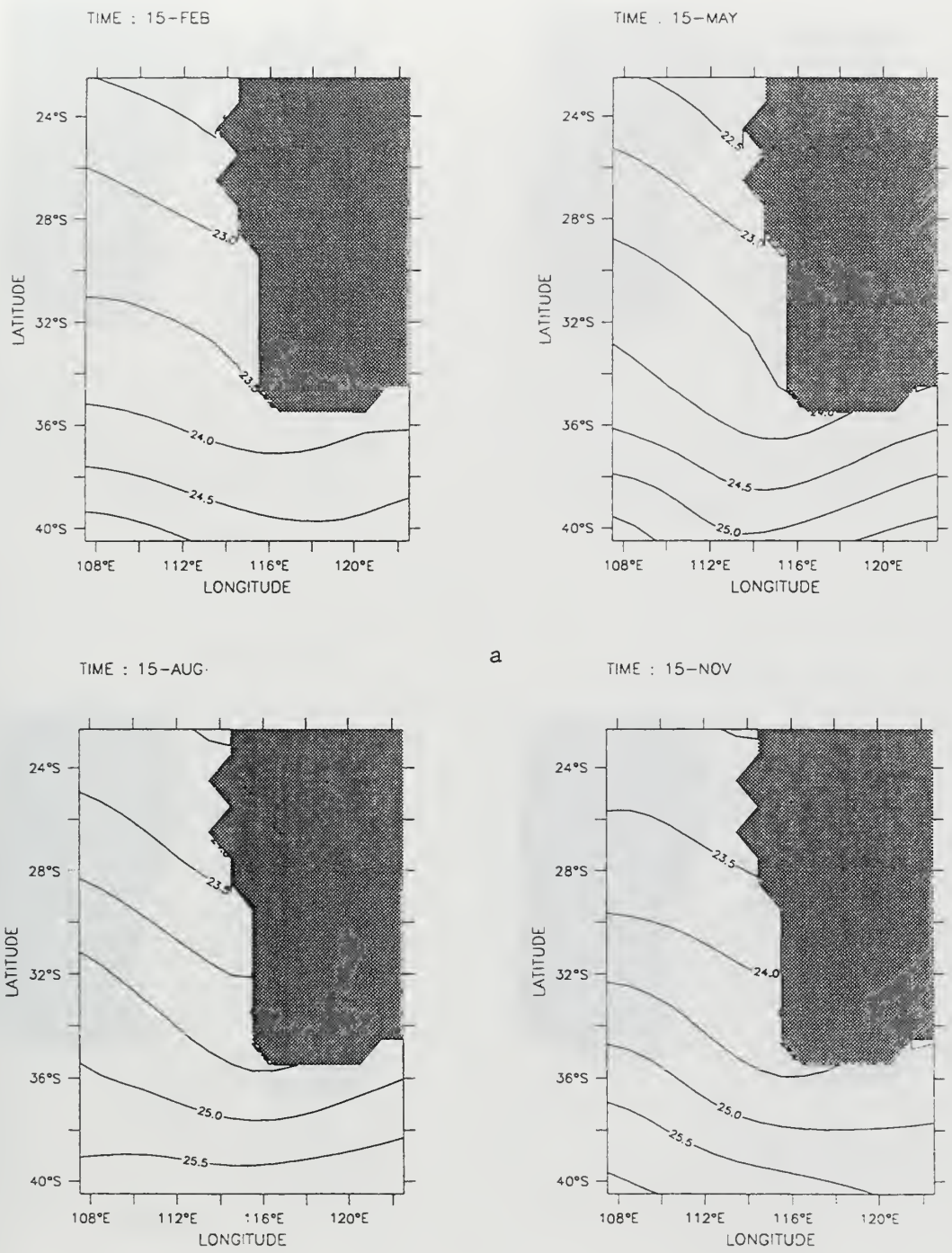

Figure 6. Seasonal density (σ_t) fields with constant (a) and variable (b) salinity at 10 m depth in February, May, August, and November. The contour interval is 0.5

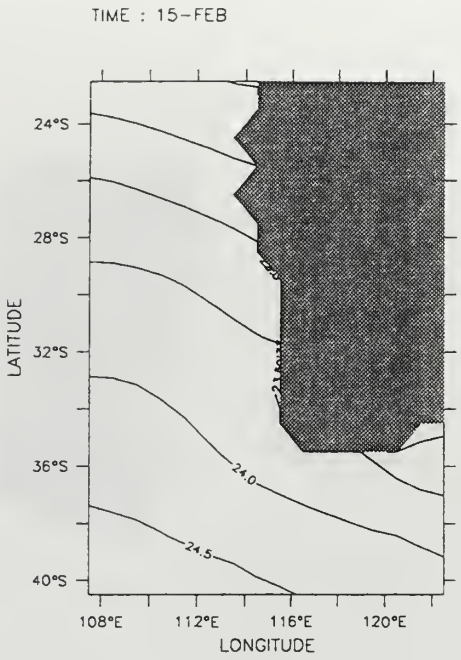
TIME : 15-FEB
24°S
28°S
32°S
36°S
40°S
LATITUDE
108°E
112°E
116°E
120°E
LONGITUDE
24.0
24.5

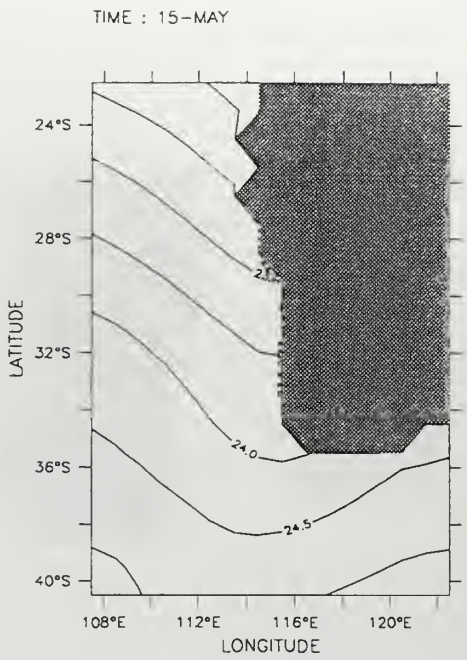
TIME : 15-MAY
24°S
28°S
32°S
36°S
40°S
LATITUDE
108°E
112°E
116°E
120°E
LONGITUDE
24.0
24.5

b

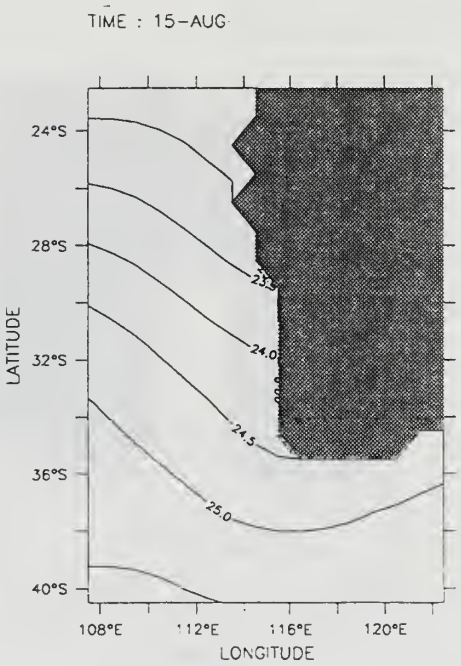
TIME : 15-AUG
24°S
28°S
32°S
36°S
40°S
LATITUDE
108°E
112°E
116°E
120°E
LONGITUDE
24.0
24.5
25.0

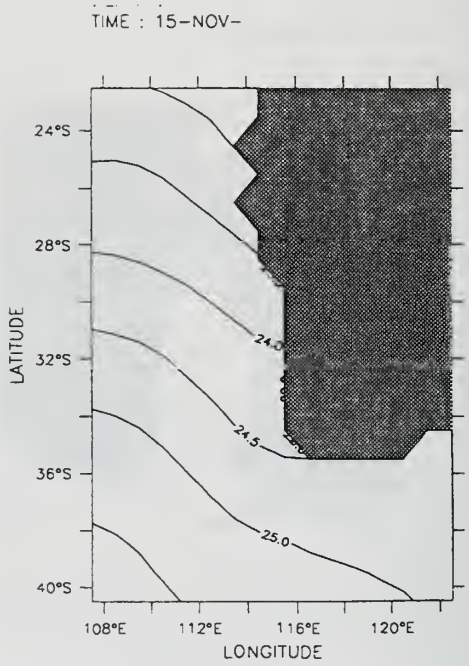
TIME : 15-NOV-
24°S
28°S
32°S
36°S
40°S
LATITUDE
108°E
112°E
116°E
120°E
LONGITUDE
24.5
25.0

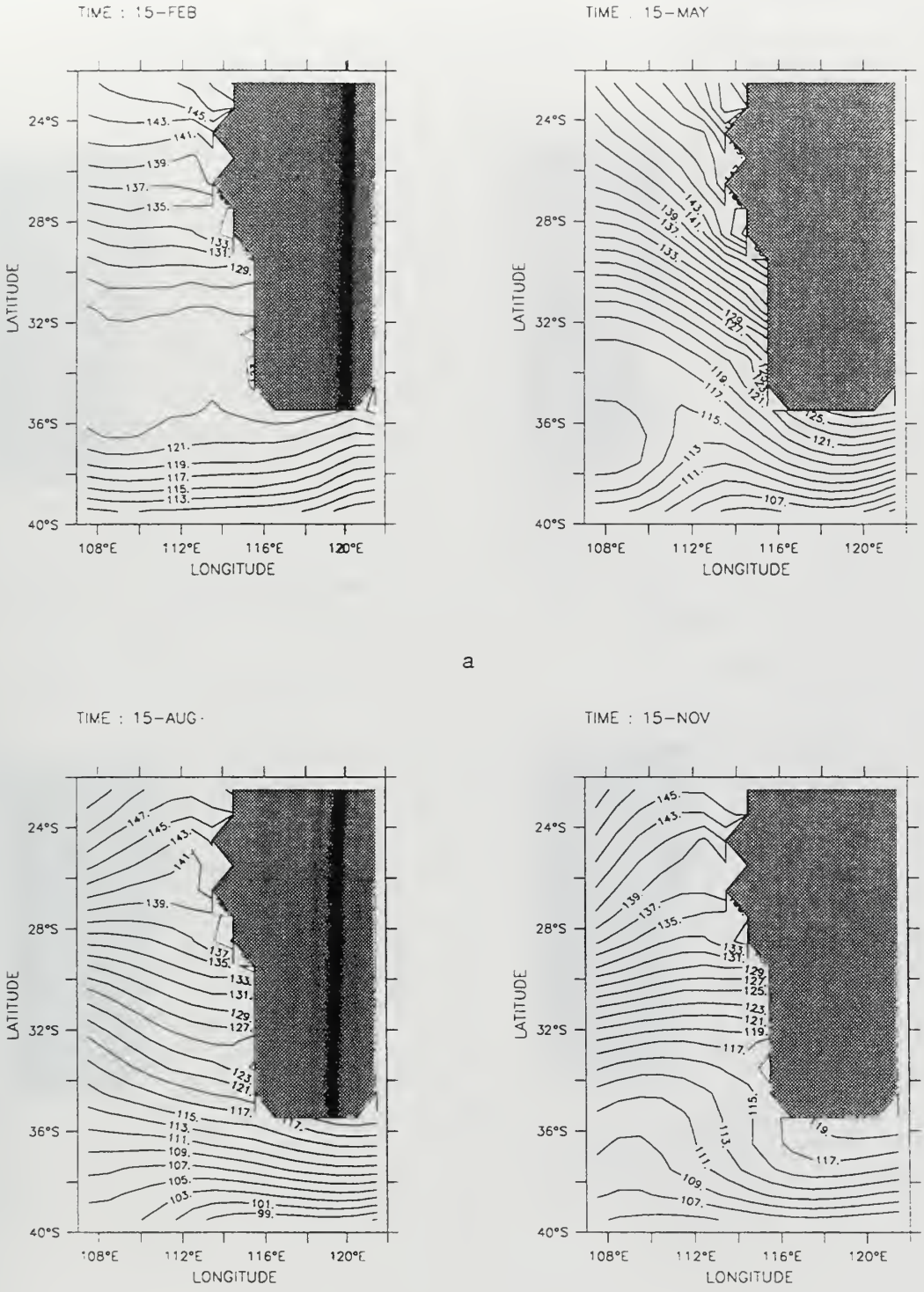

a

Figure 7. Seasonal dynamic height fields with constant (a) and variable (b) salinity at 10 m depth in February, May, August, and November. The contour interval is 2 dyn. cm.

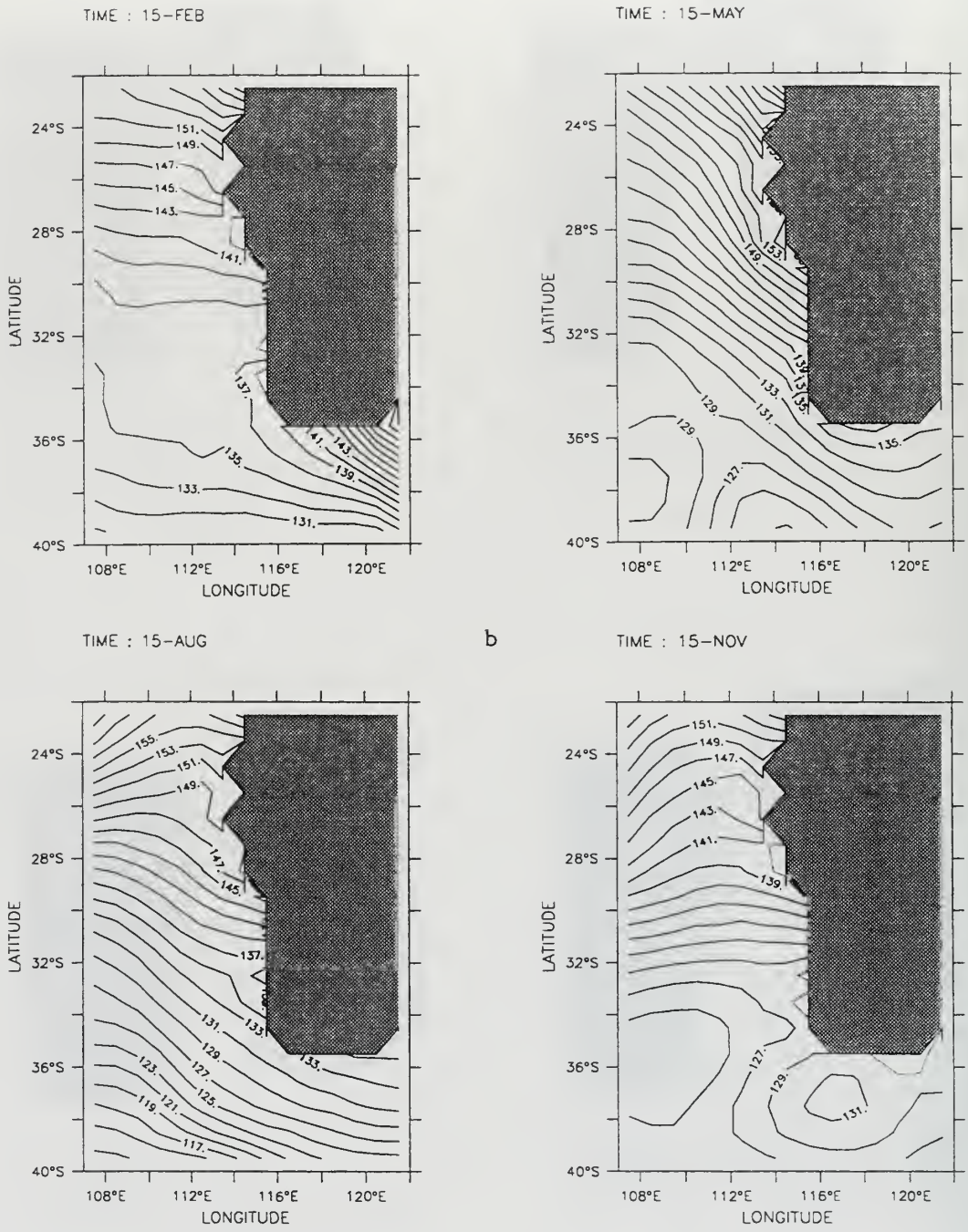
TIME : 15-FEB
TIME : 15-MAY
TIME : 15-AUG
TIME : 15-NOV
LATITUDE
LONGITUDE
24°S
28°S
32°S
36°S
40°S
108°E
112°E
116°E
120°E

b

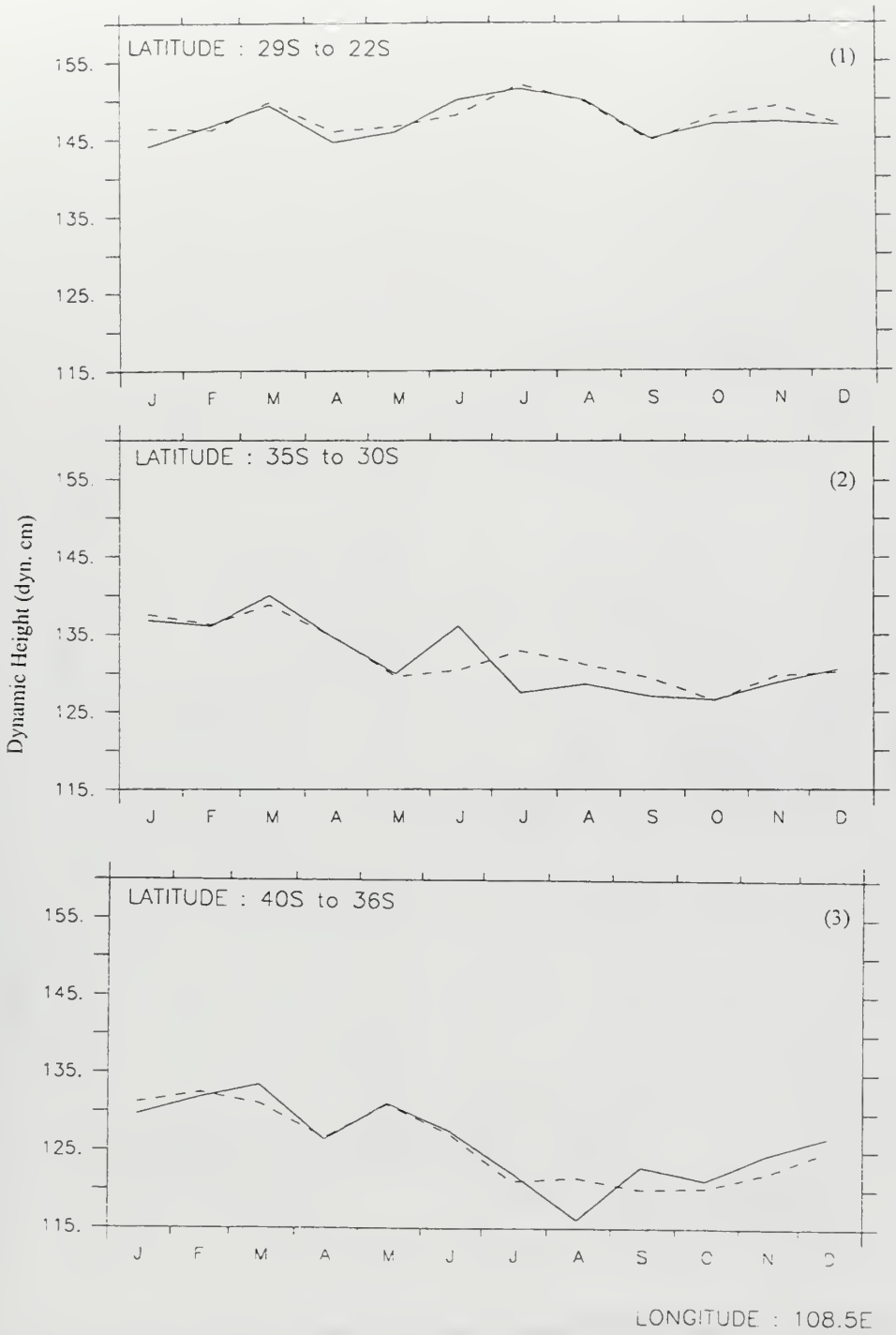

Figure 8. Seasonal dynamic height fields meridionally averaged at 108.5°E from (1) 22.5°S to 29°S; (2) 30°S to 35°S; and (3) 36°S to 40°S. The dashed (solid) line refers to dynamic height calculated with constant (variable) salinity.

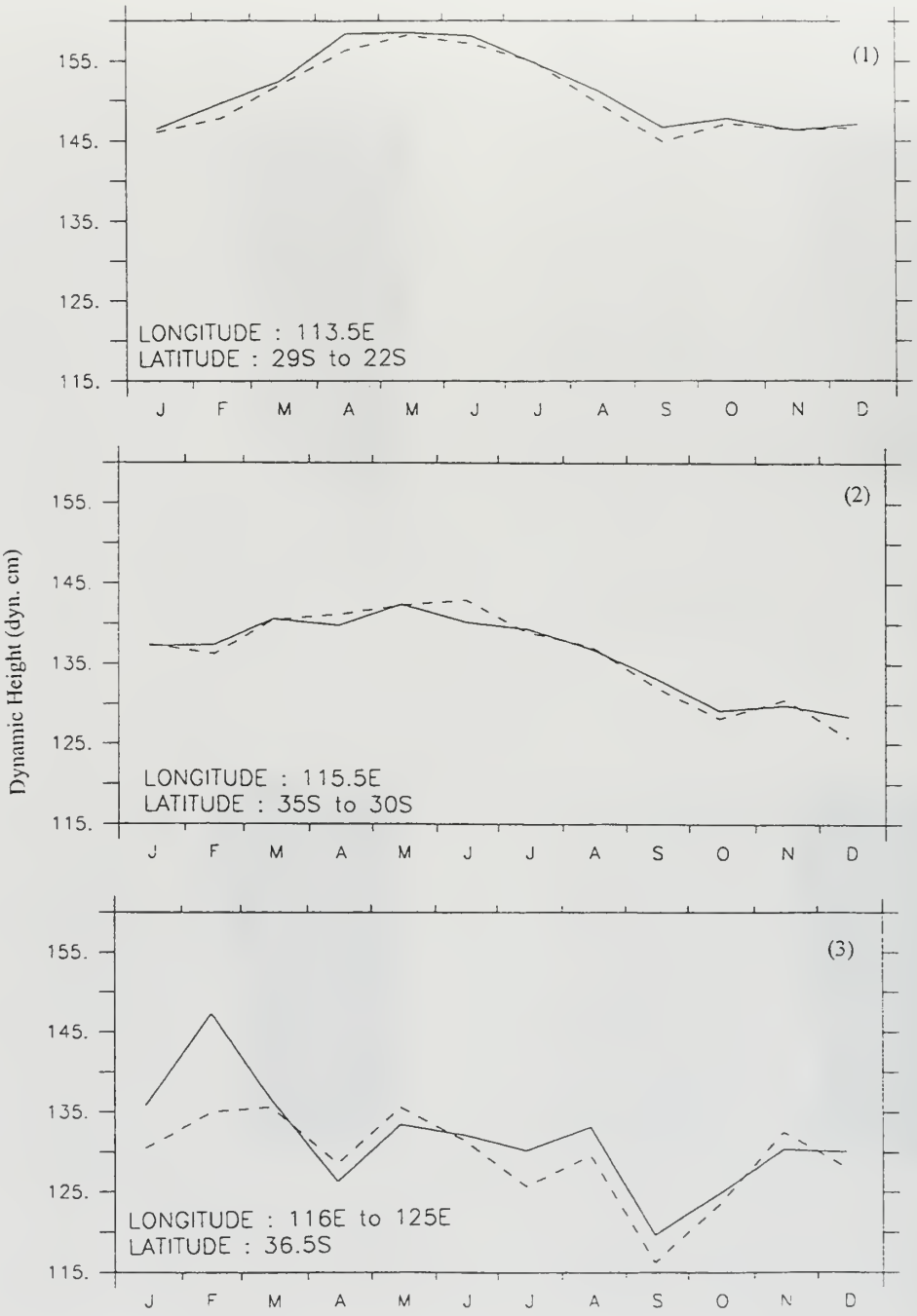

Figure 9. Seasonal dynamic height fields in the nearshore region at (1) 113.5°E, which is latitudinally averaged from 22°S to 29°S; (2) 115.5°E, which is latitudinally averaged from 30°S to 35°S; (3) and 36.5°S, which is longitudinally averaged from 116°E to 125°E. The dashed (solid) line refers to dynamic height calculated with constant (variable) salinity.

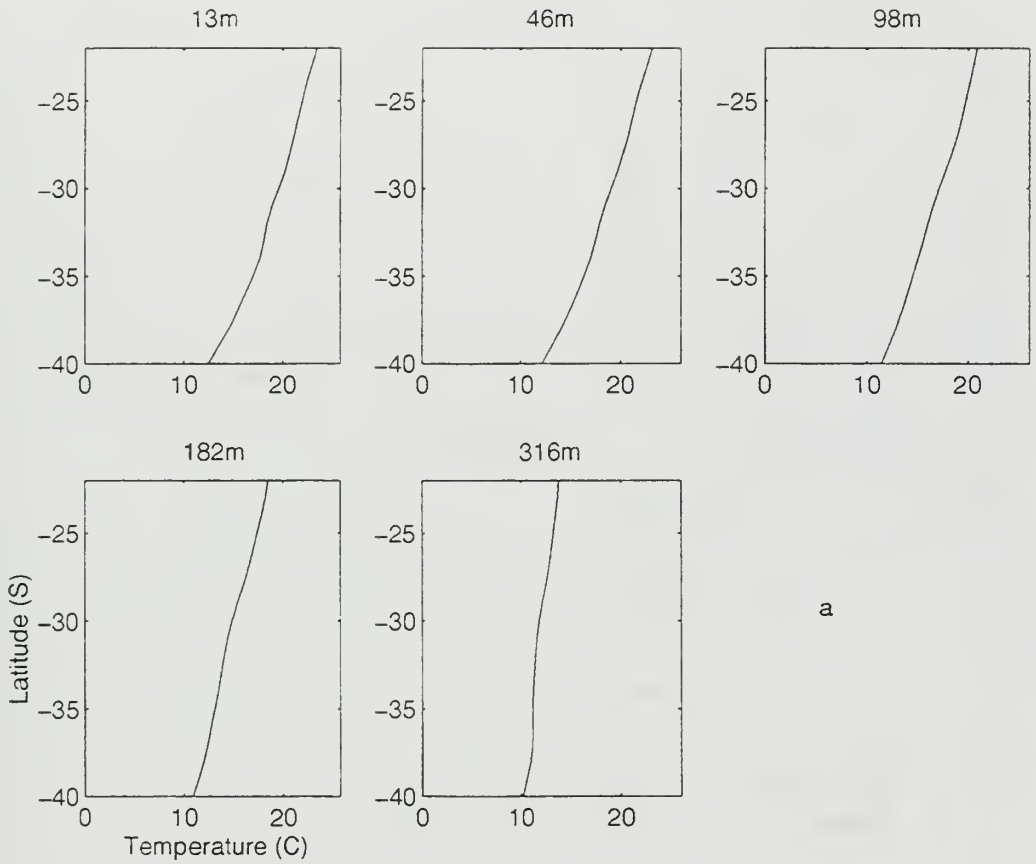

Figure 10. The annual temperature (a) and salinity (b) field forcing conditions for the upper five levels. Since the lower five levels do not have much latitudinal variation, they are assumed to be constant for each level.

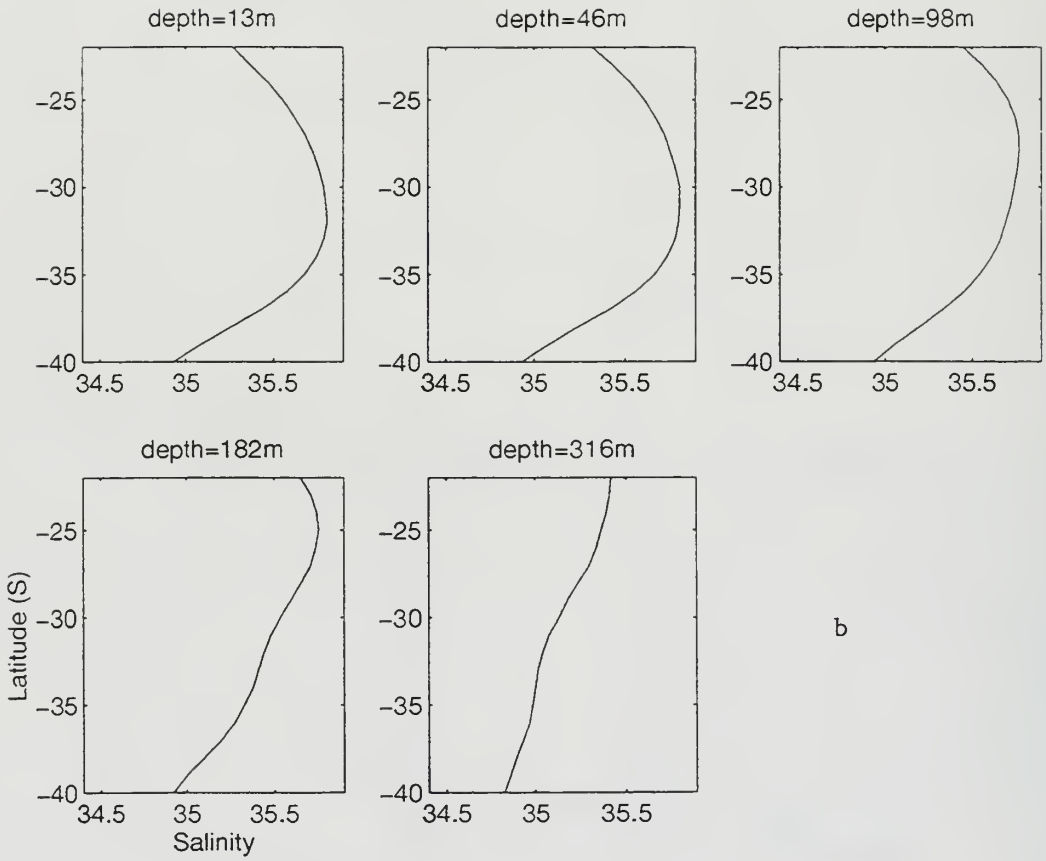
depth=13m
depth=46m
depth=98m
depth=182m
depth=316m
-25
-30
-35
-40
34.5
35
35.5
Latitude (S)
Salinity

b

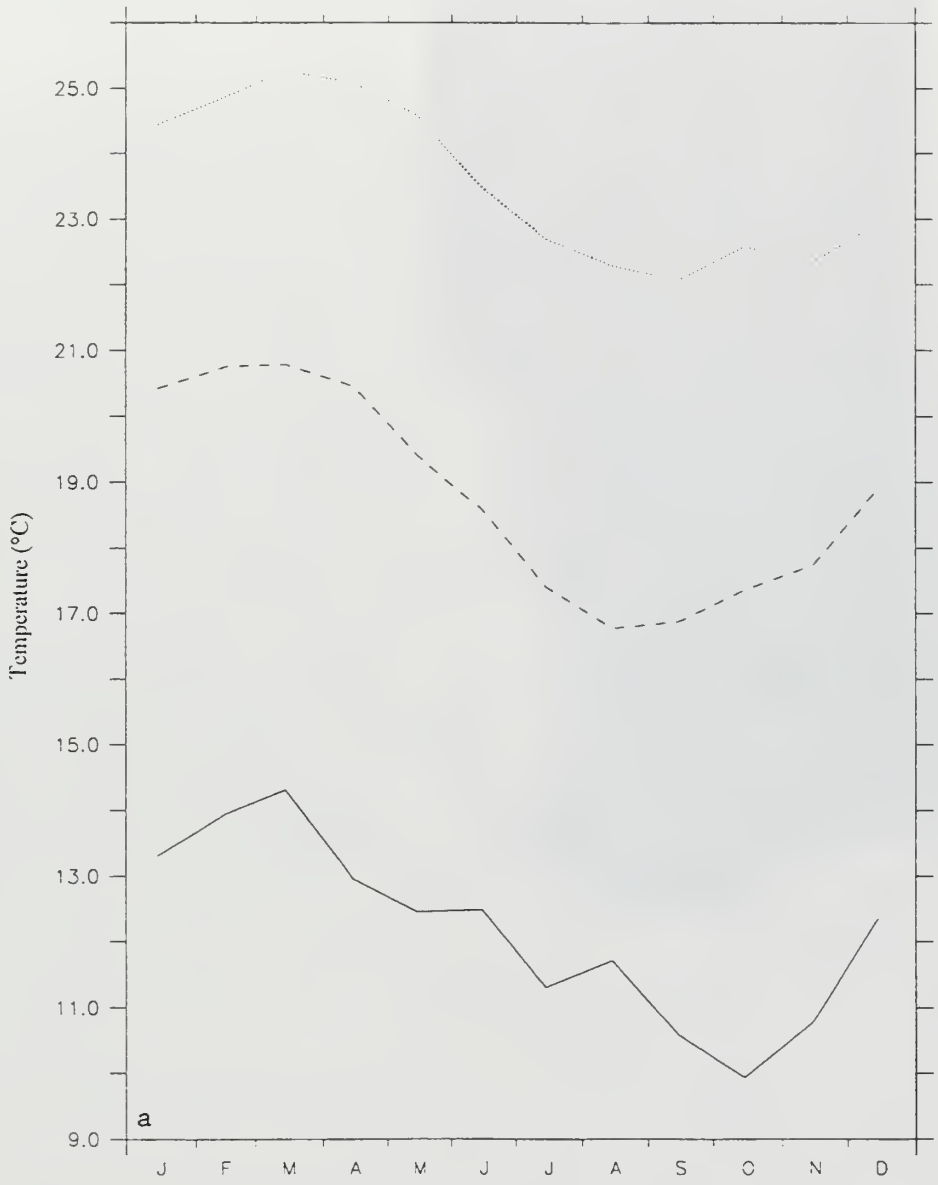

Figure 11 Time series plot at 10 m depth of monthly temperature (a) and salinity (b) fields used as seasonal forcing in Experiments 3 and 4. The solid lines are for 40°S, the dashed lines for 31.5°S, and the dotted lines for 22.5°S.

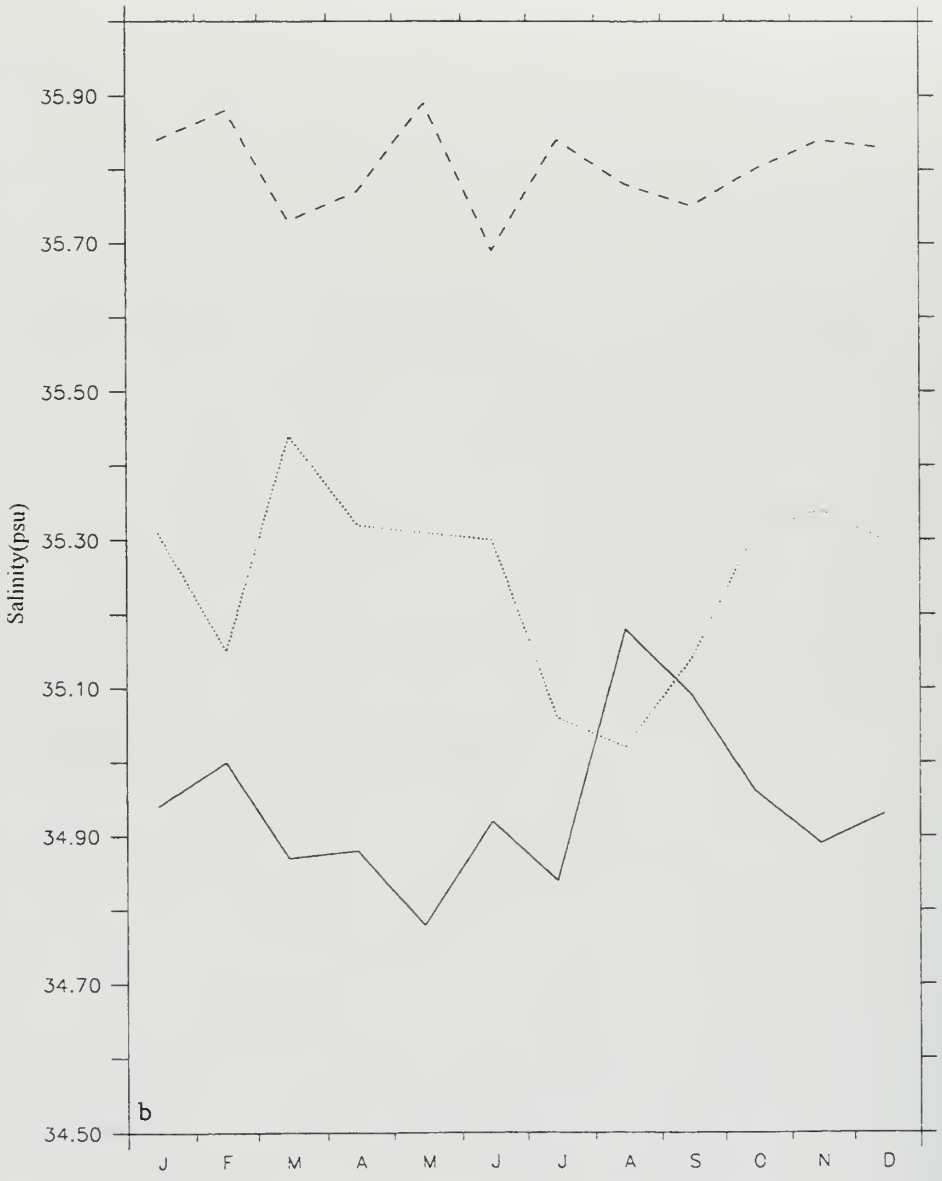
35.90
35.70
35.50
35.30
35.10
34.90
34.70
34.50
Salinity(psu)
b
J
F
M
A
M
J
J
A
S
O
N
D

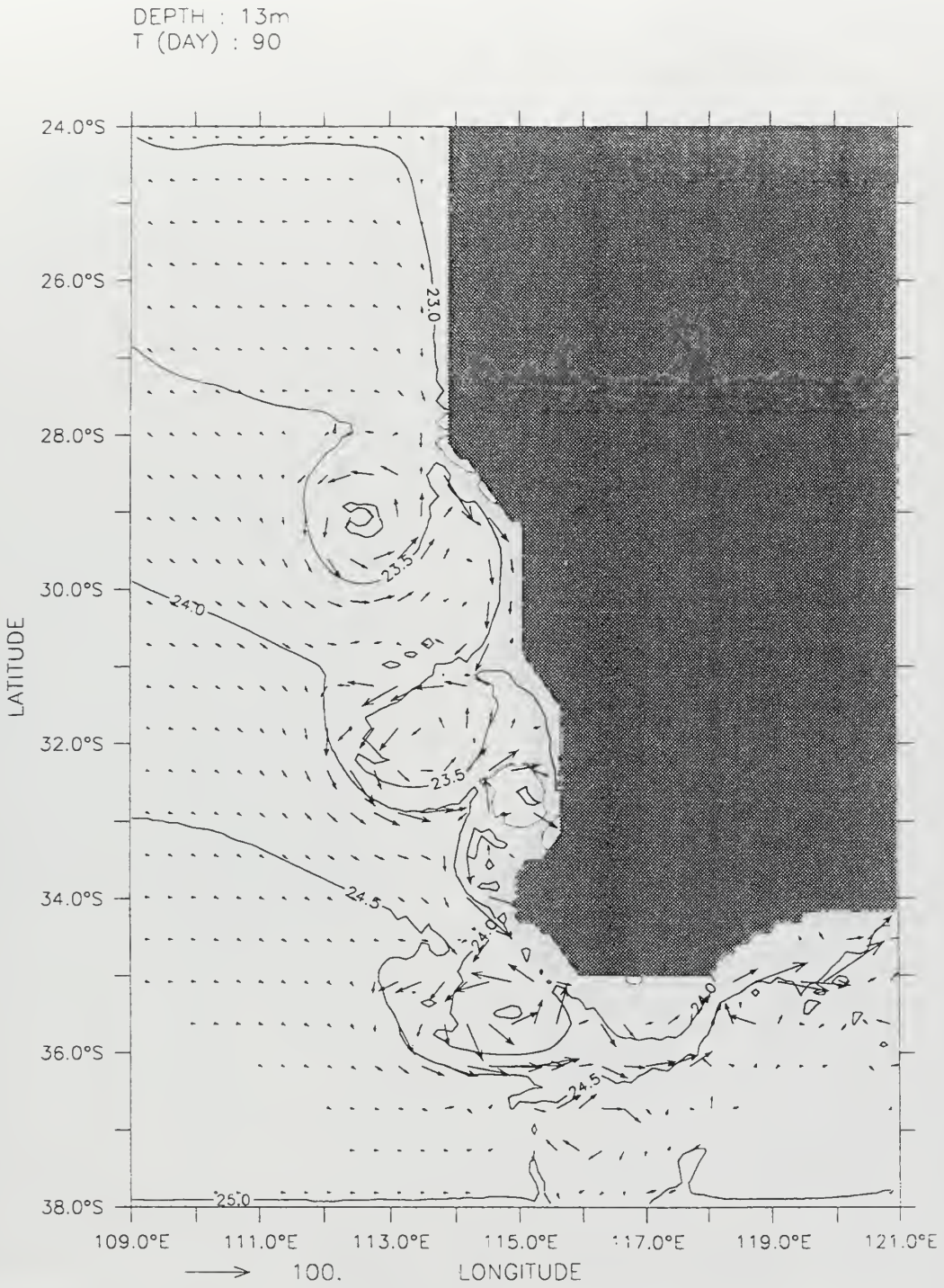

Figure 12. Experiment 1 surface density (σ_t) field and velocity vectors at day 90. In this and the following figures, to avoid clutter, velocity vectors are plotted at every fourth grid point in the alongshore and cross-shore directions. The contour interval is 0.5.

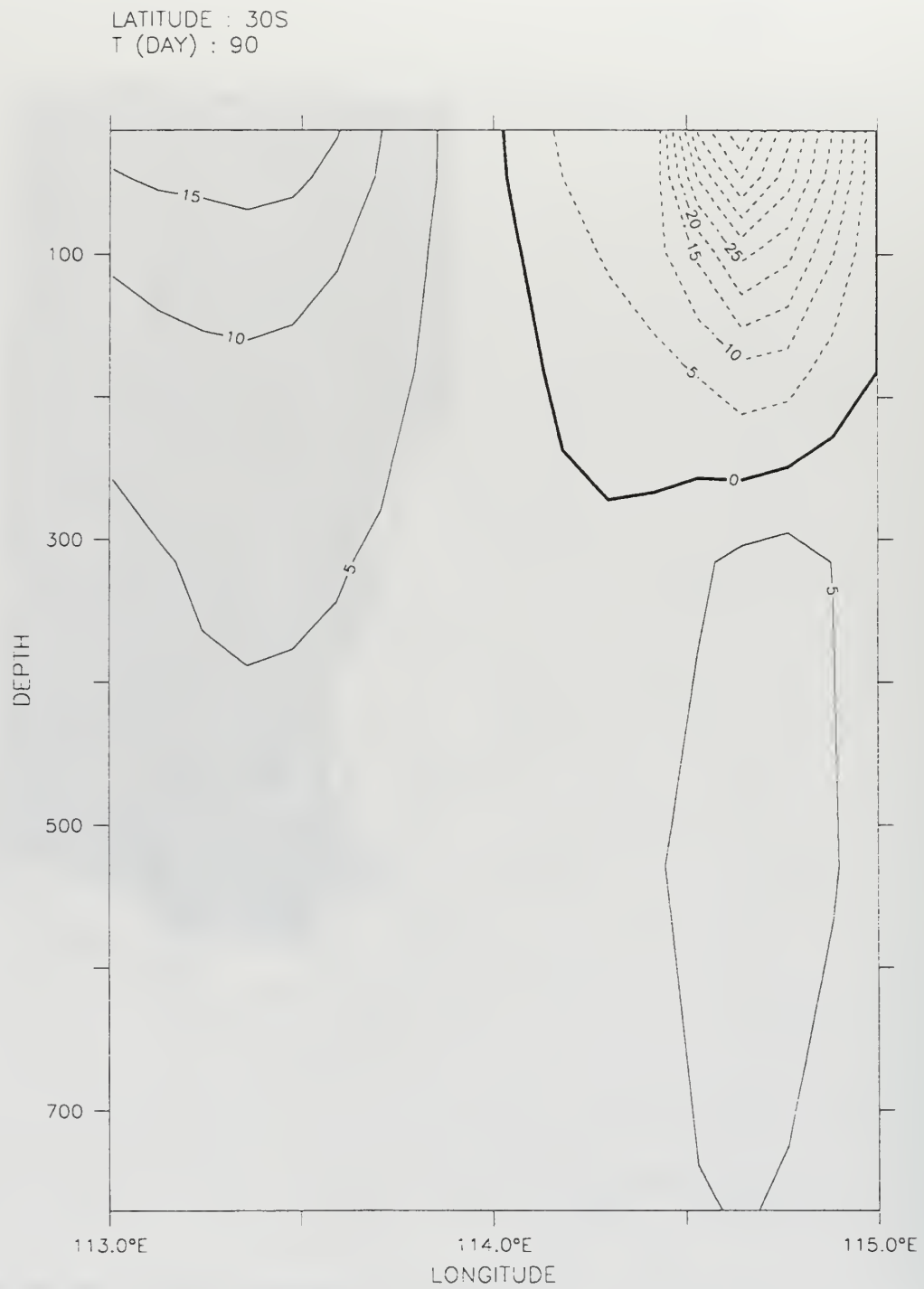

Figure 13. Cross-shore section of velocity field for Experiment 1 at day 90. Solid lines indicate equatorward flow, while dashed lines indicate poleward flow. The contour interval is 5 cm/s.

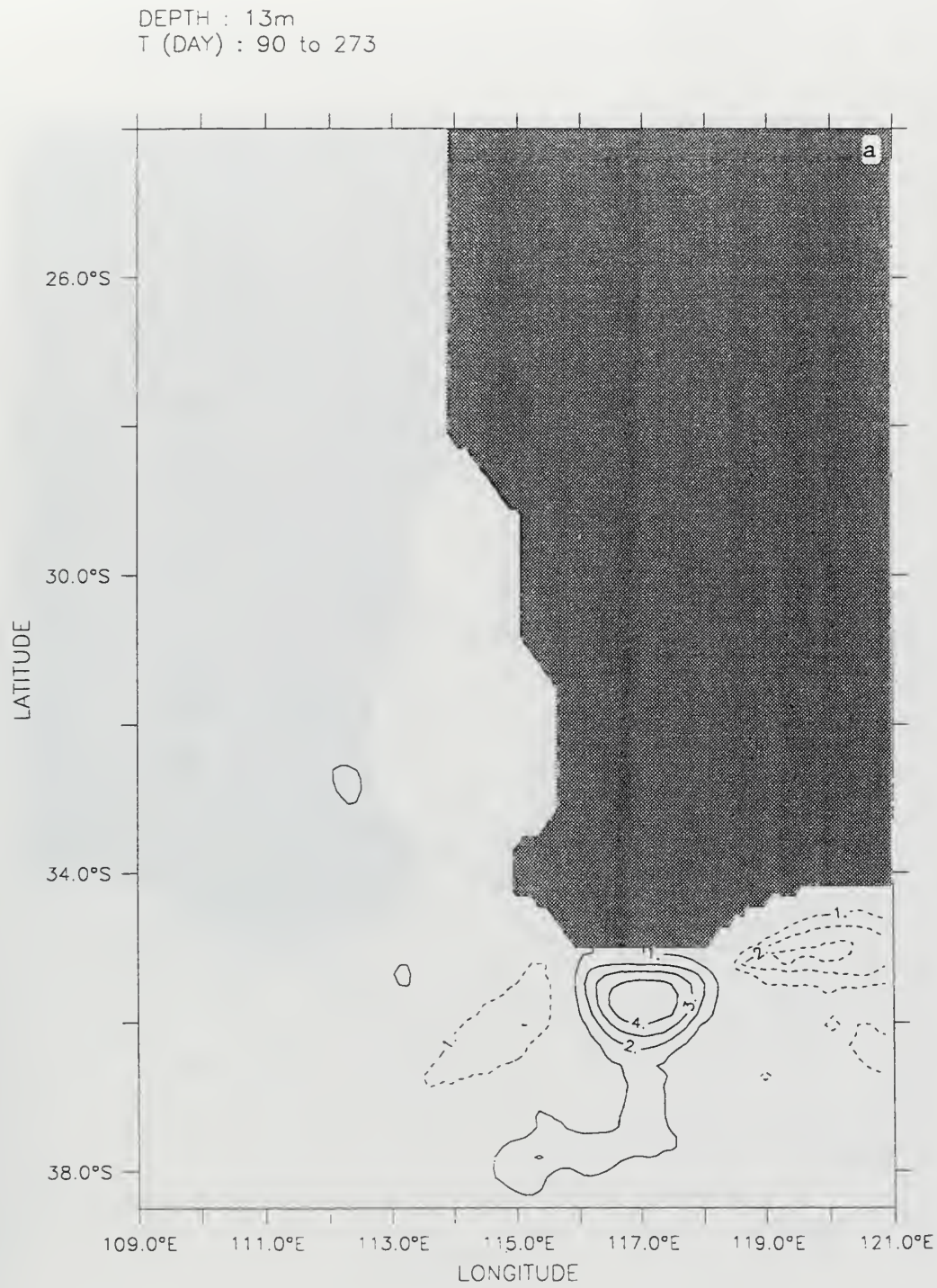

Figure 14. Difference of time-averaged temperature (a) and density (b) from April to September (days 90-273) between annual forcing experiments with variable (Experiment 1) and constant (Experiment 2) salinity. The contour interval is 1°C in (a) and 0.1 in (b).

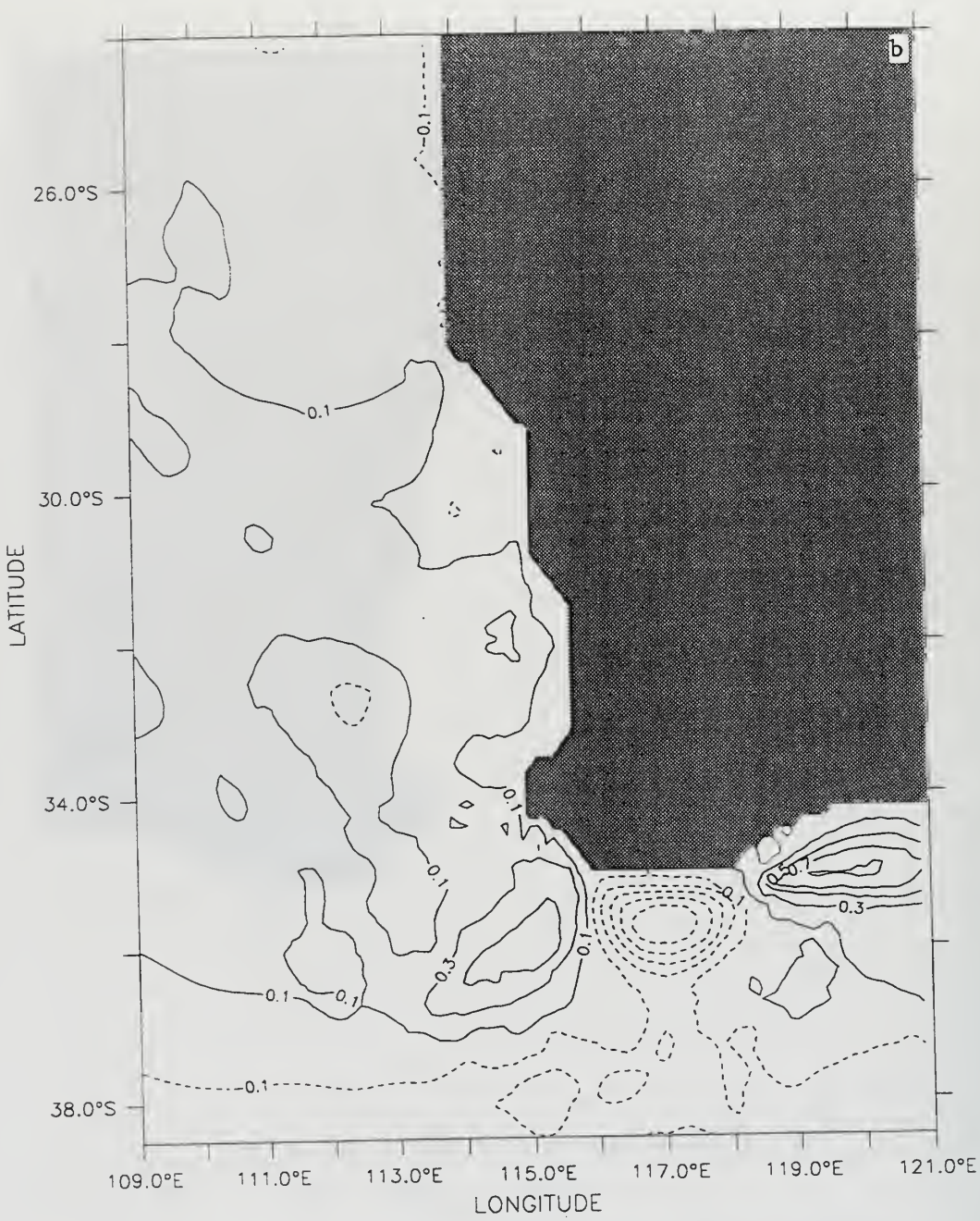
DEPTH : 13m
T (DAY) : 90 to 273
b
26.0°S
30.0°S
34.0°S
38.0°S
LATITUDE
109.0°E
111.0°E
113.0°E
115.0°E
117.0°E
119.0°E
121.0°E
LONGITUDE
0.1
0.3

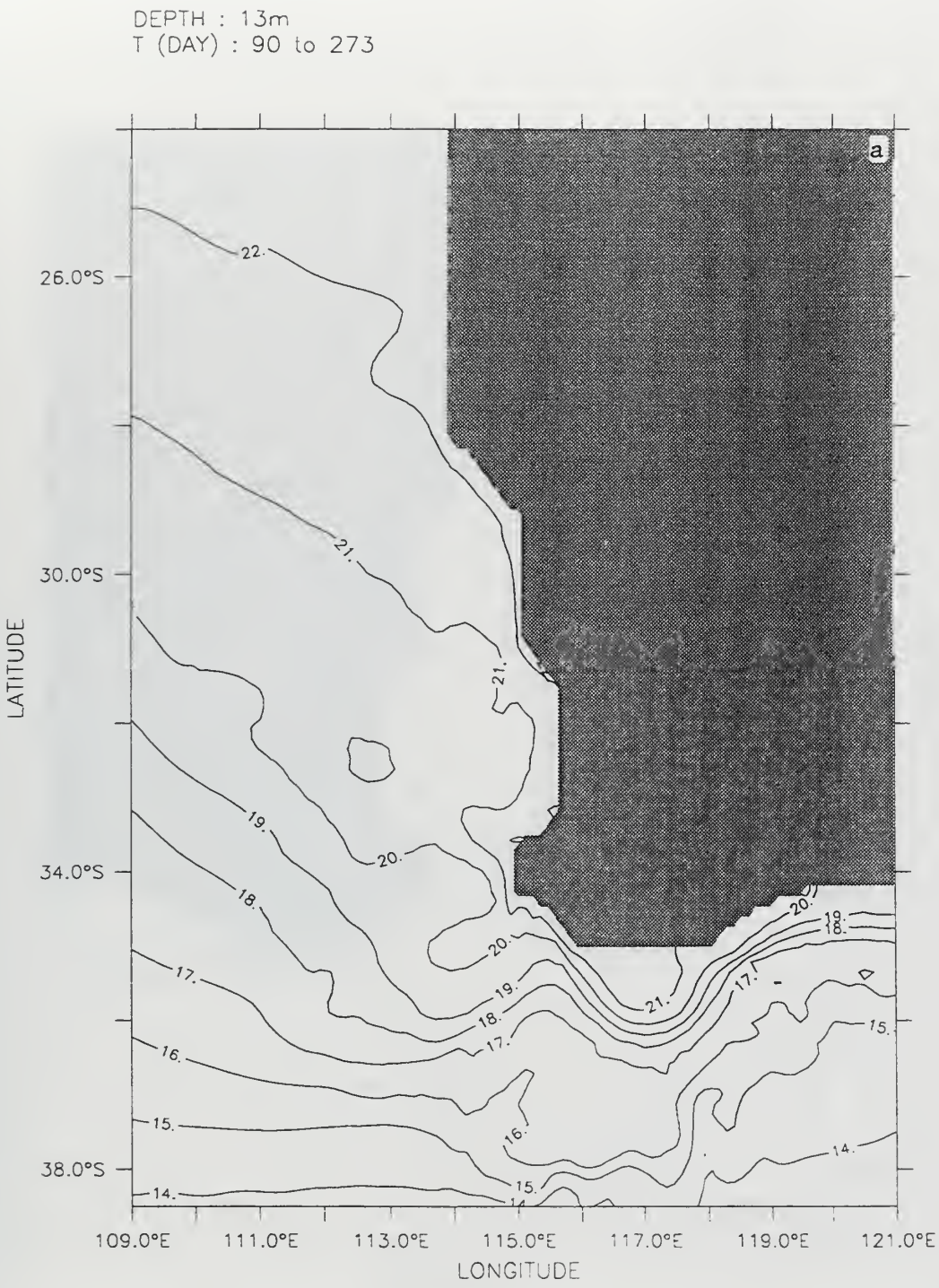

Figure 15. Time-averaged temperature fields from April to September (days 90-273) for (a) Experiment 1 and (b) Experiment 2. The contour interval is 1°C.

DEPTH : 13m
T (DAY) : 90 to 273

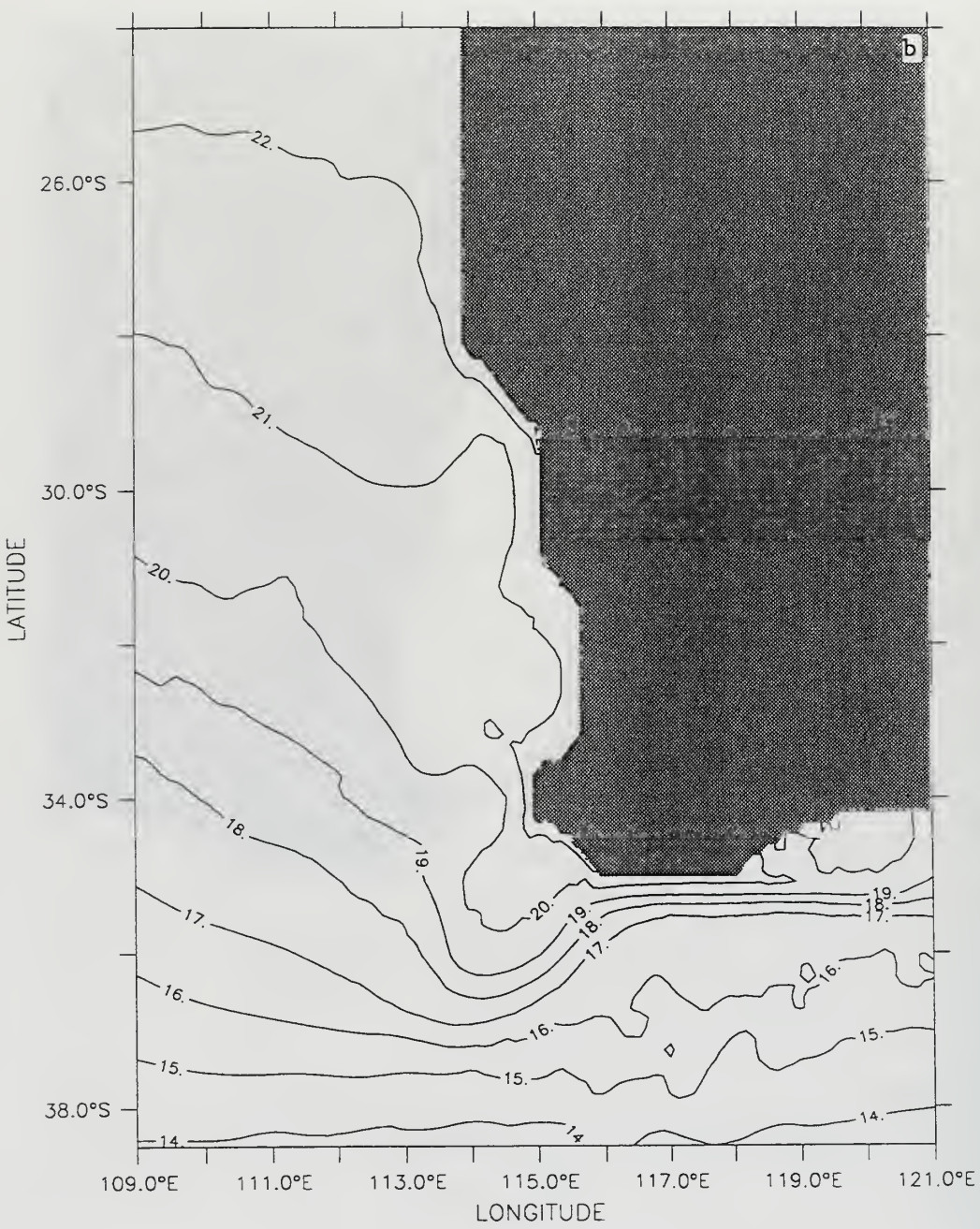

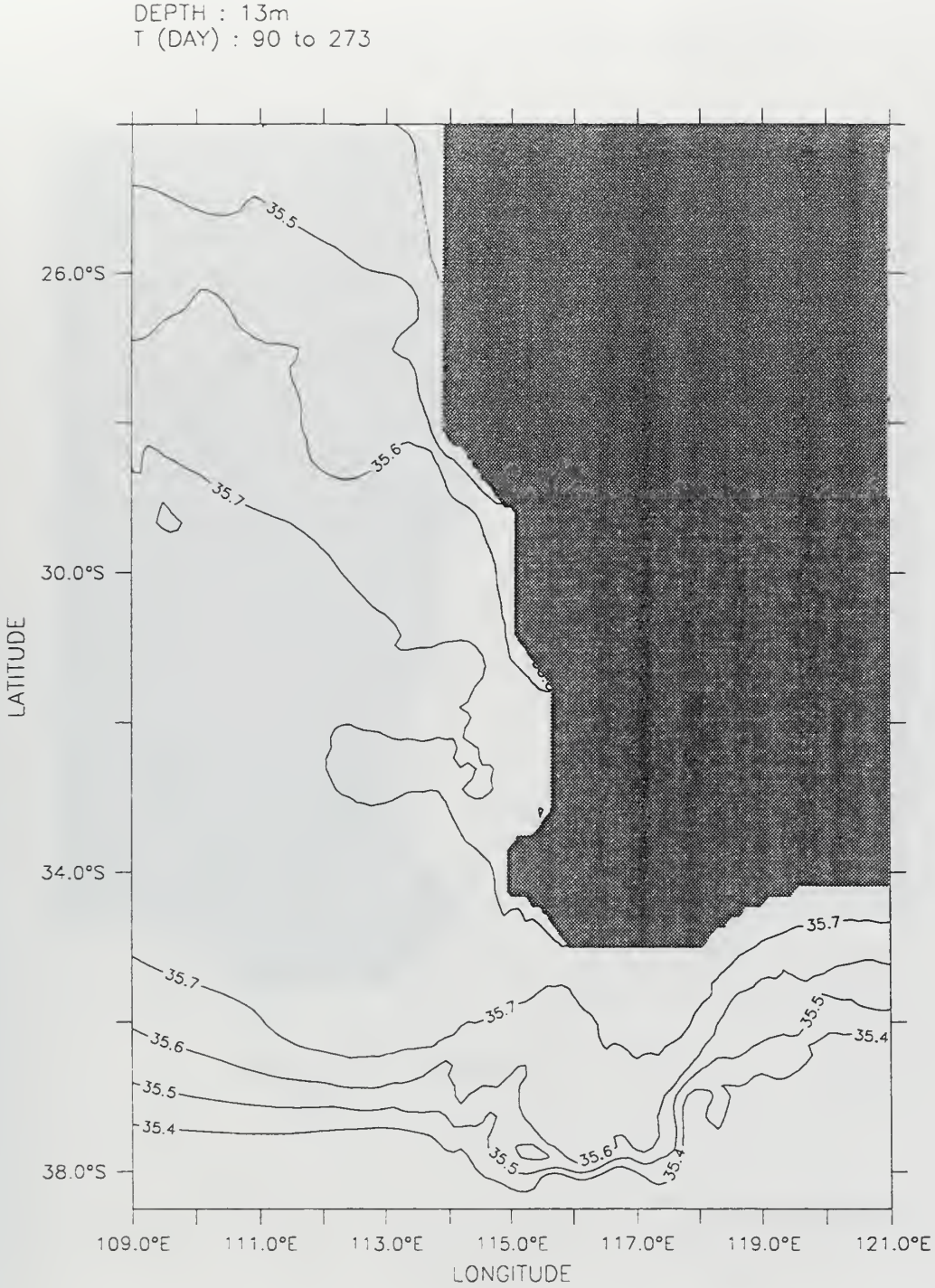

Figure 16. Experiment 1 time-averaged salinity fields from April to September (days 90-273). The contour interval is 0.1 psu.

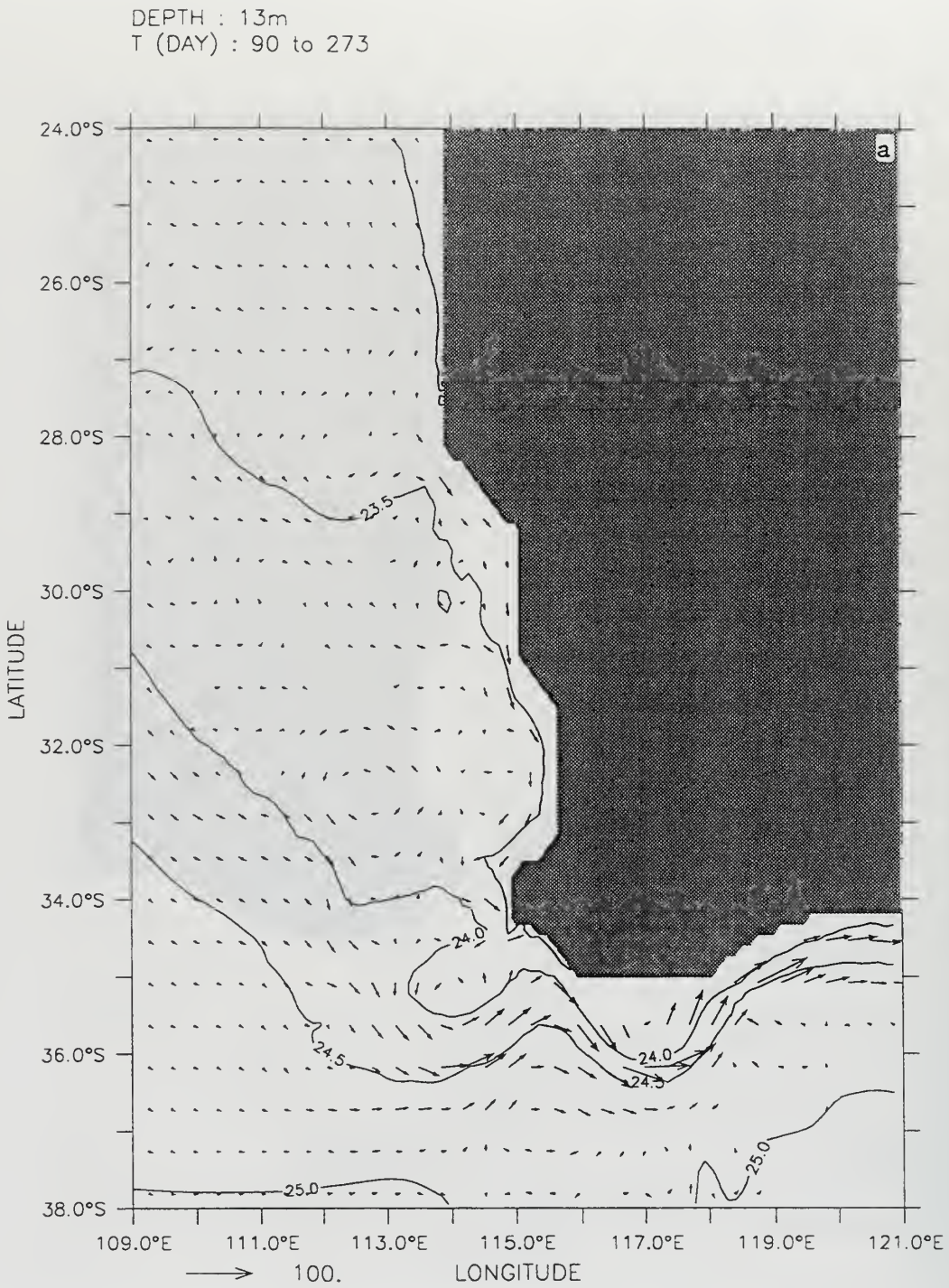

Figure 17. Time-averaged density (σ_t) fields and velocity vectors from April to September (days 90-273) for (a) Experiment 1 and (b) Experiment 2. The contour interval is 0.5.

DEPTH : 13m
T (DAY) : 90 to 273

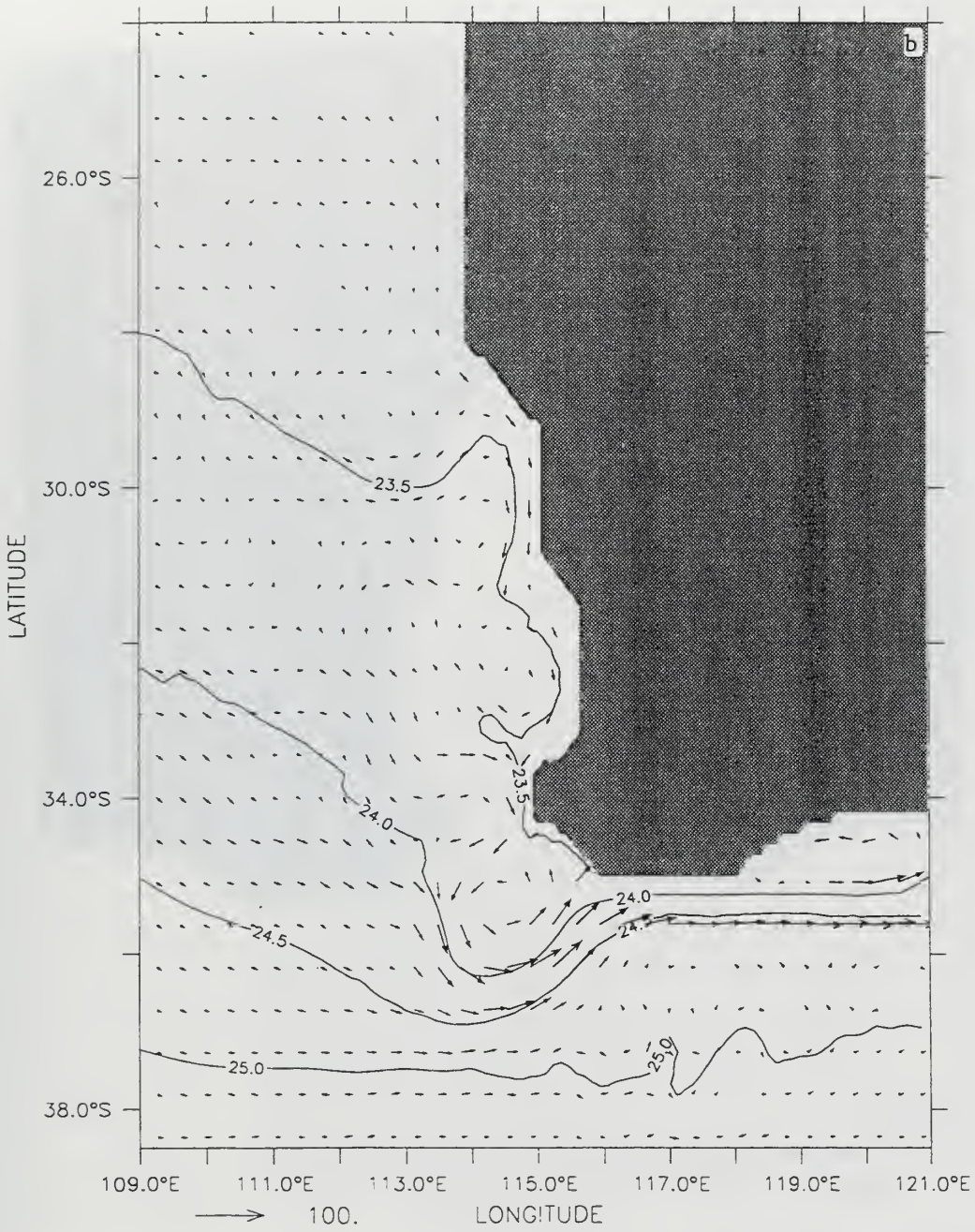

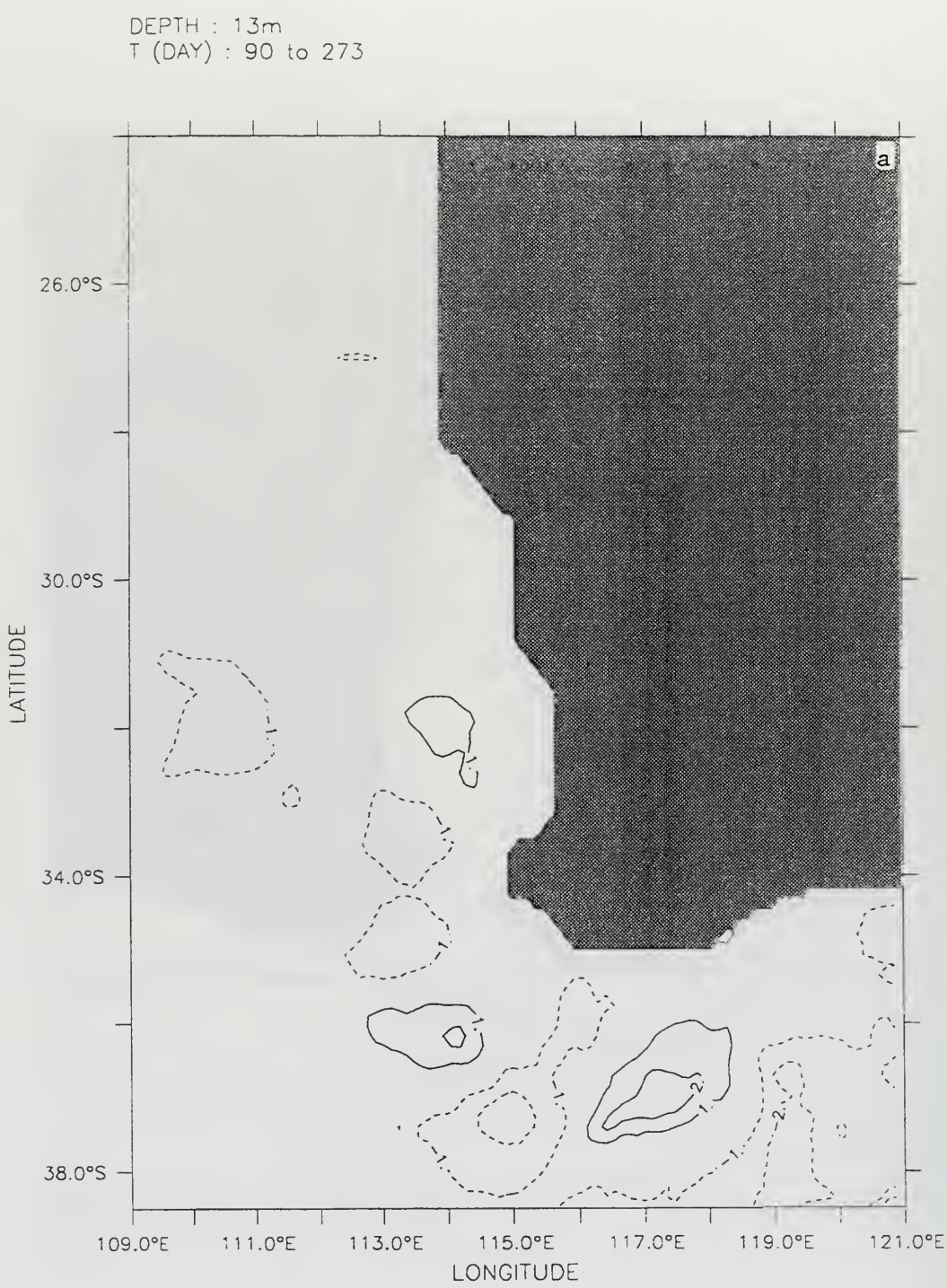

Figure 18. Difference of time-averaged temperature (a) and density (σ_t) (b) fields from April to September (days 90-273) between annual forcing experiments with variable (Experiment 3) and constant (Experiment 4) salinity. The contour interval is 1°C in (a) and 0.1 in (b).

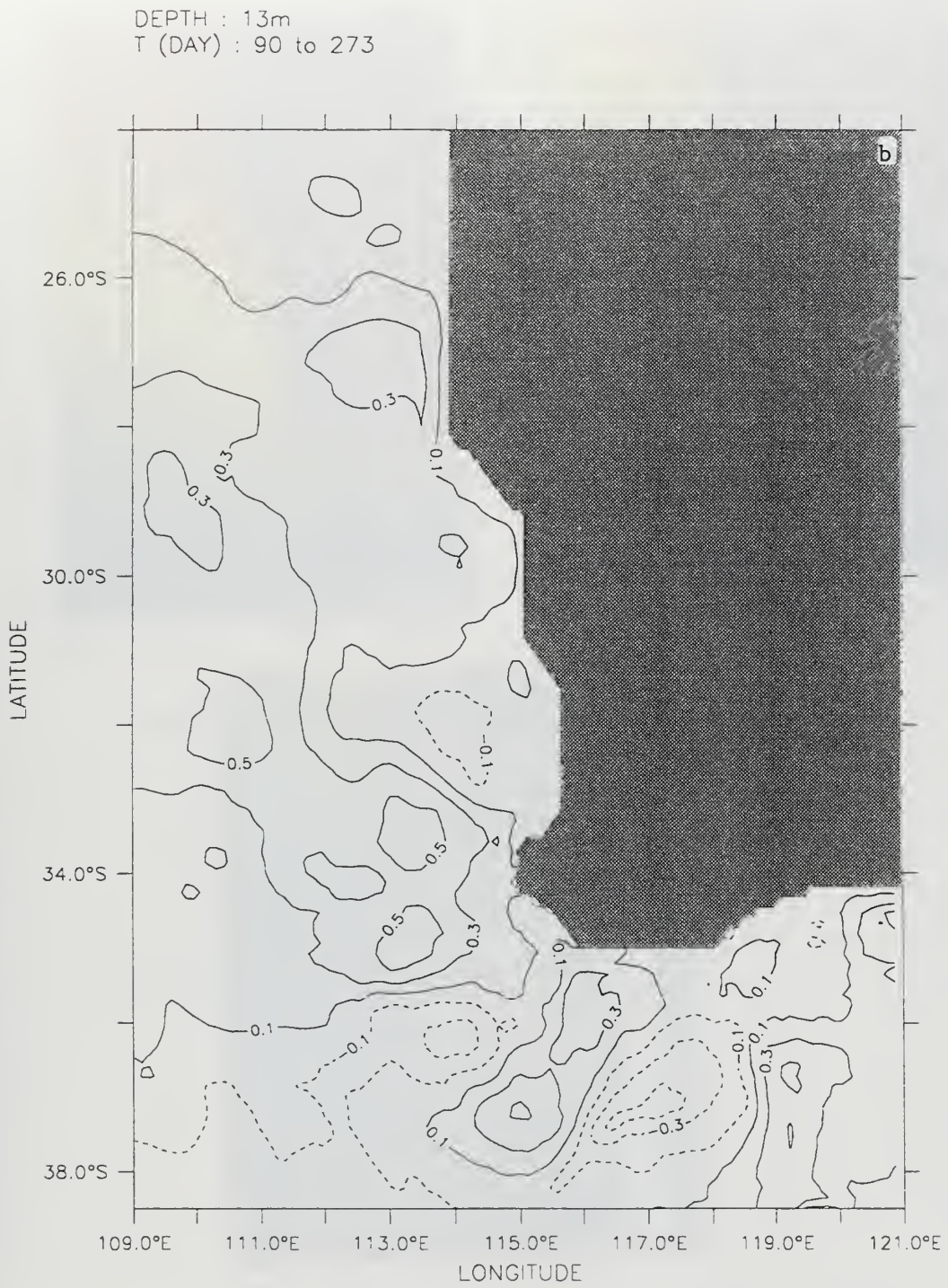
DEPTH : 13m
T (DAY) : 90 to 273
b
26.0°S
30.0°S
34.0°S
38.0°S
LATITUDE
109.0°E
111.0°E
113.0°E
115.0°E
117.0°E
119.0°E
121.0°E
LONGITUDE
0.3
0.1
0.5
-0.1
-0.3

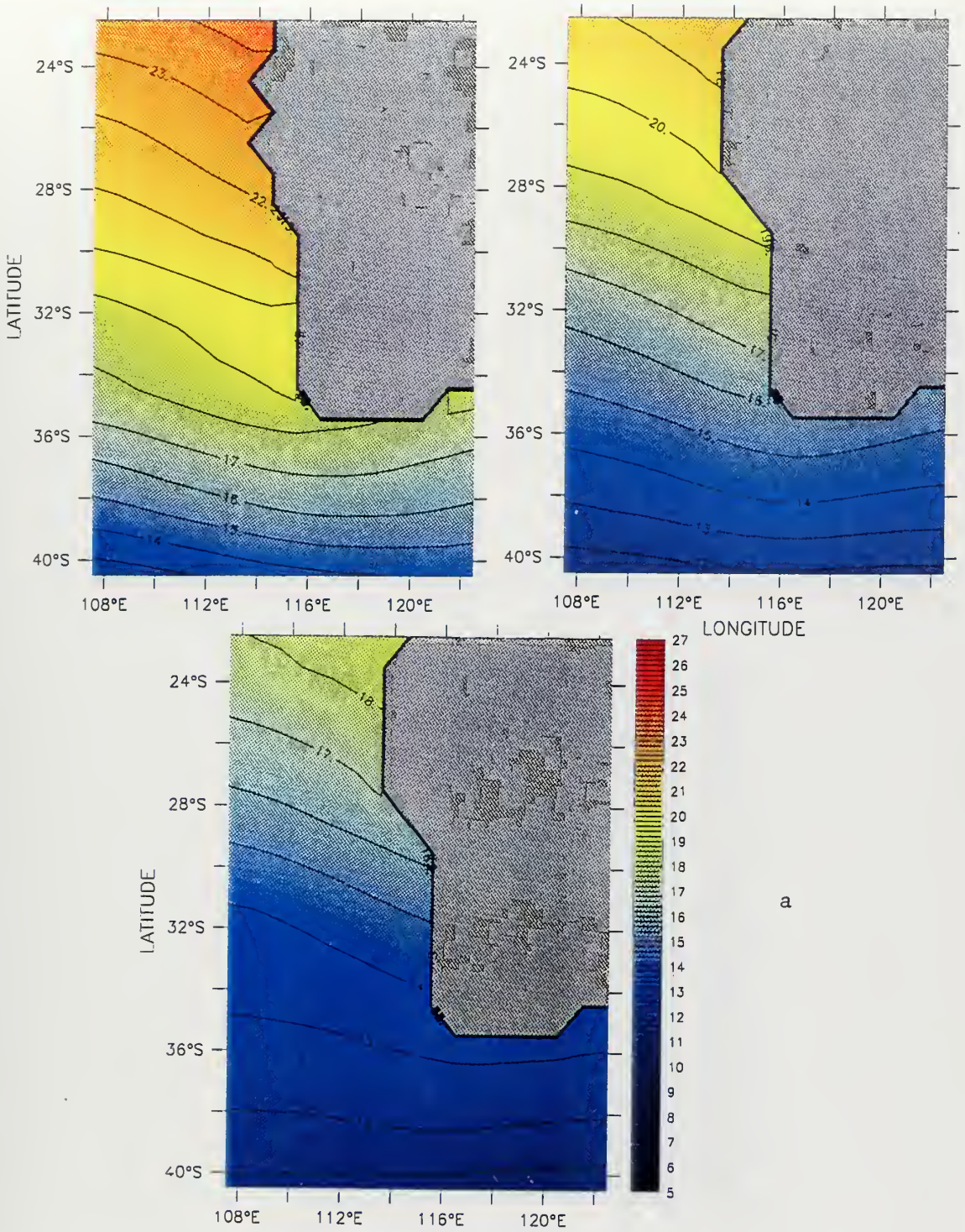

Plate 1. Climatological annual mean temperature (a) and salinity (b) fields at 10, 100, and 200 m depth. Note that the coastline differentiates with depth. Annual density fields with constant (c) variable (d) salinity at 10, 100, and 200 m depth.

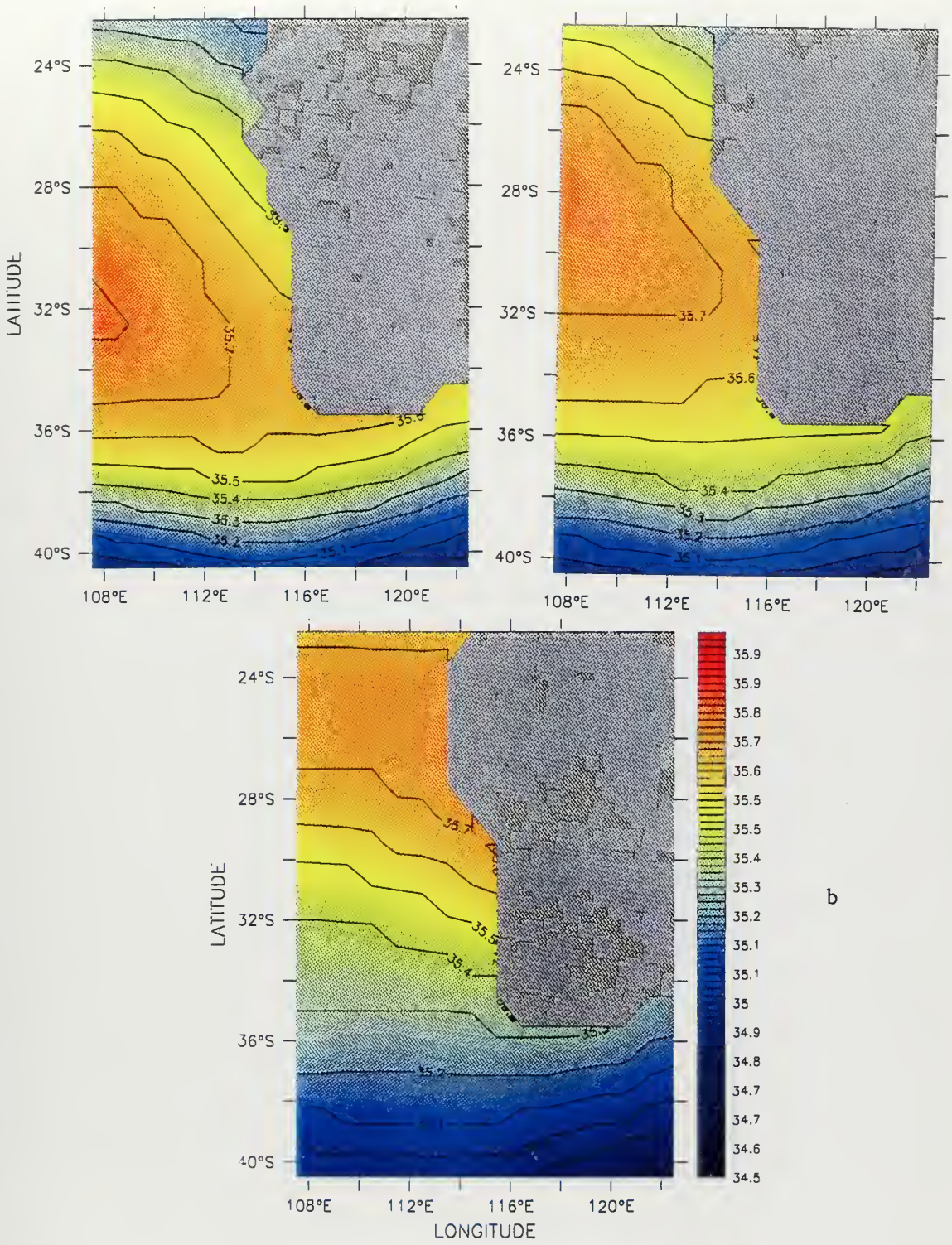
24°S
28°S
32°S
36°S
40°S
LATITUDE
108°E
112°E
116°E
120°E
LONGITUDE
35.7
35.6
35.5
35.4
35.3
35.2
35.1
35.9
35.9
35.8
35.7
35.6
35.5
35.5
35.4
35.3
35.2
35.1
35.1
35
34.9
34.8
34.7
34.7
34.6
34.5

b

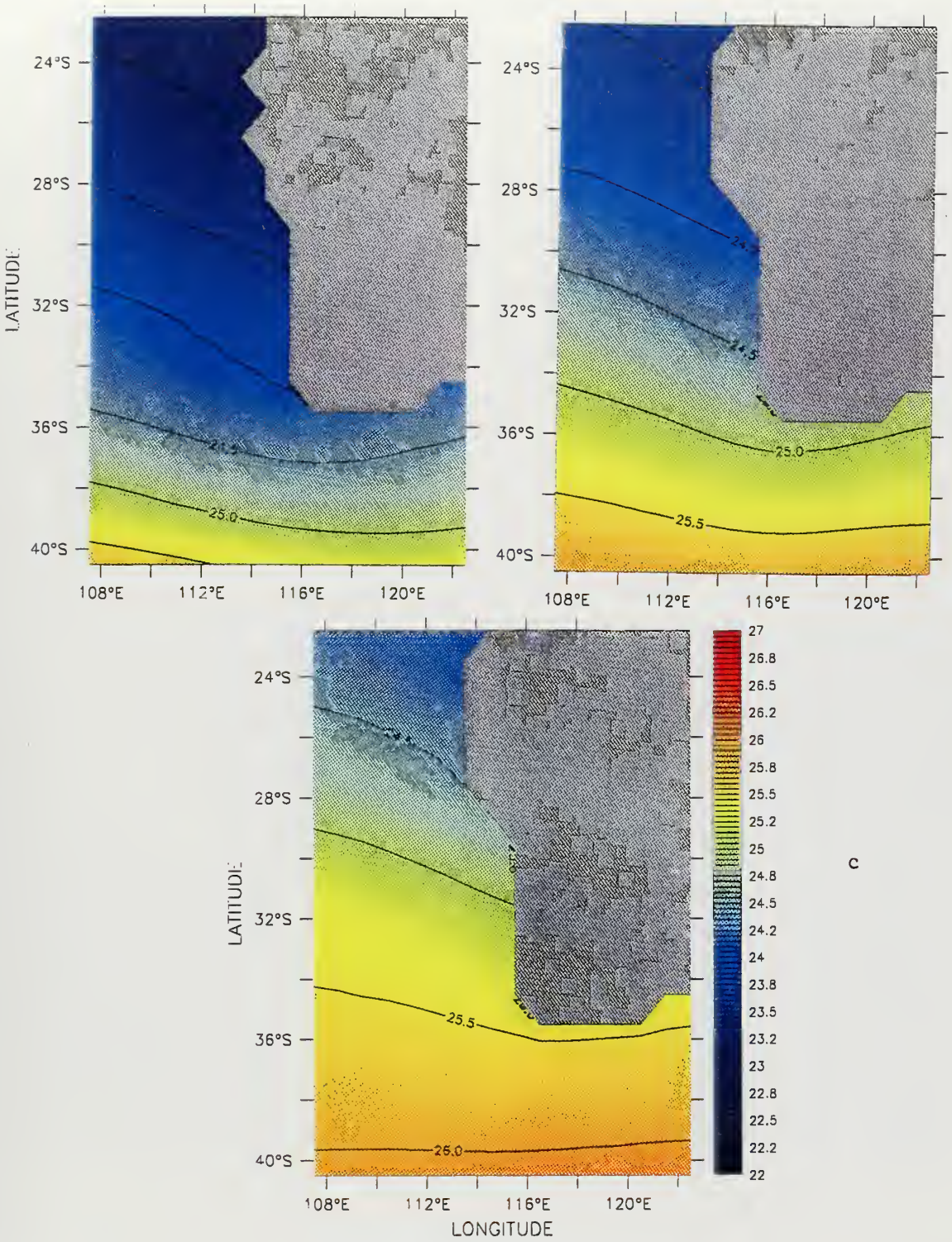
24°S
28°S
32°S
36°S
40°S
LATITUDE
108°E
112°E
116°E
120°E
LONGITUDE
25.0
25.5
27
26.8
26.5
26.2
26
25.8
25.5
25.2
25
24.8
24.5
24.2
24
23.8
23.5
23.2
23
22.8
22.5
22.2
22
c

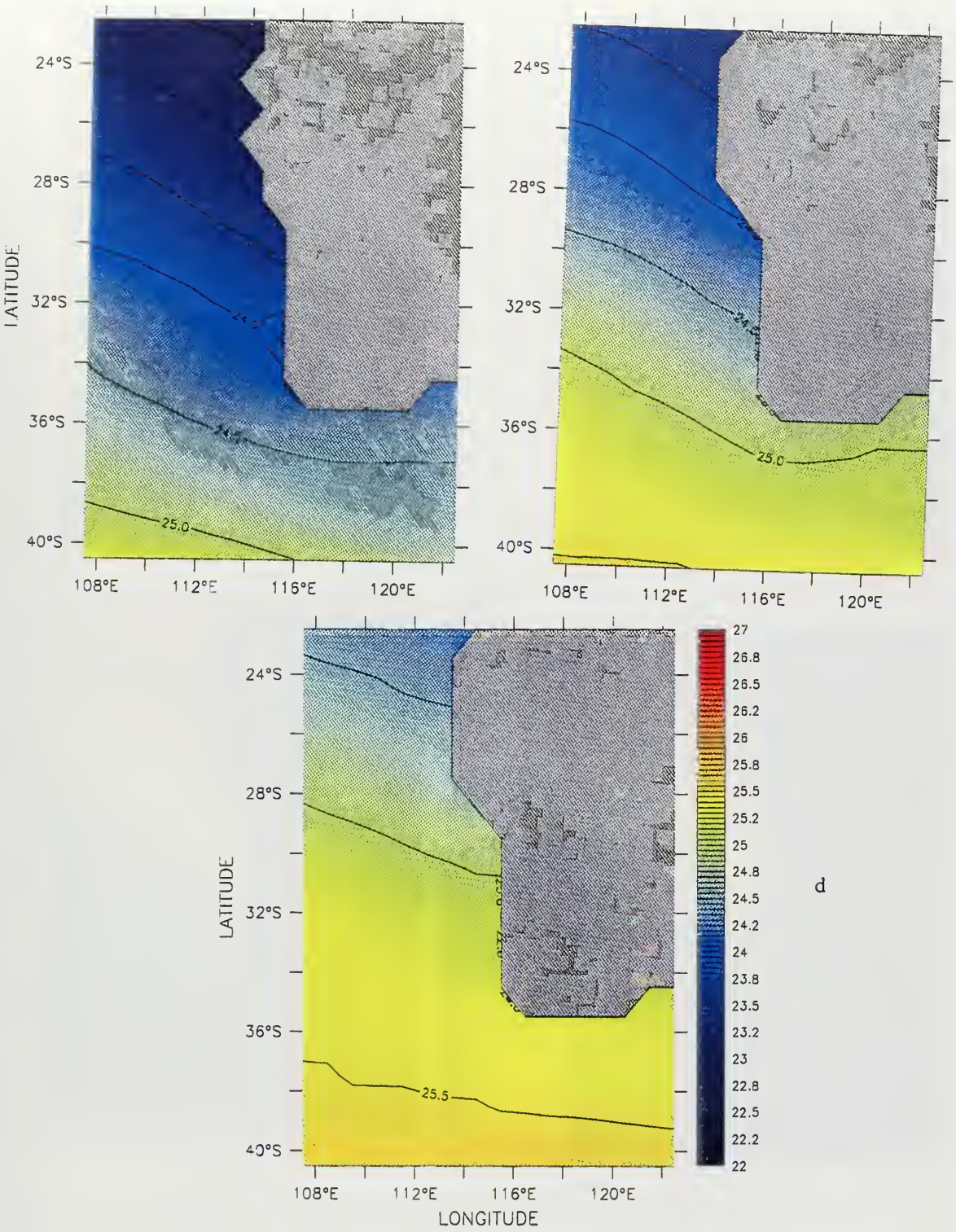
24°S
28°S
32°S
36°S
40°S
108°E
112°E
116°E
120°E
LATITUDE
LONGITUDE
25.0
25.5
27
26.8
26.5
26.2
26
25.8
25.5
25.2
25
24.8
24.5
24.2
24
23.8
23.5
23.2
23
22.8
22.5
22.2
22

d

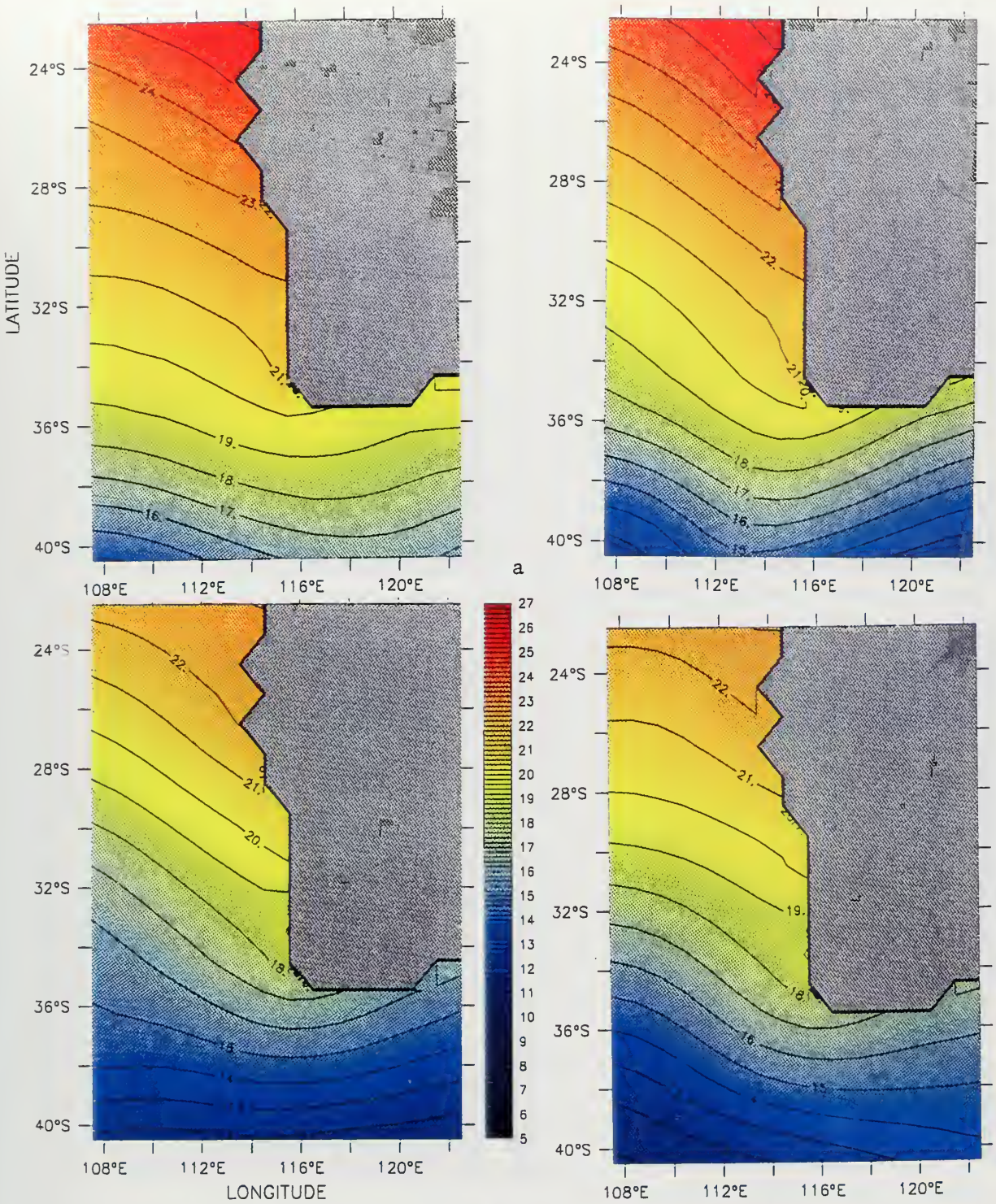

Plate 2. Climatological seasonal temperature (a) and salinity (b) fields at 10 m depth in February, May, August, and November.

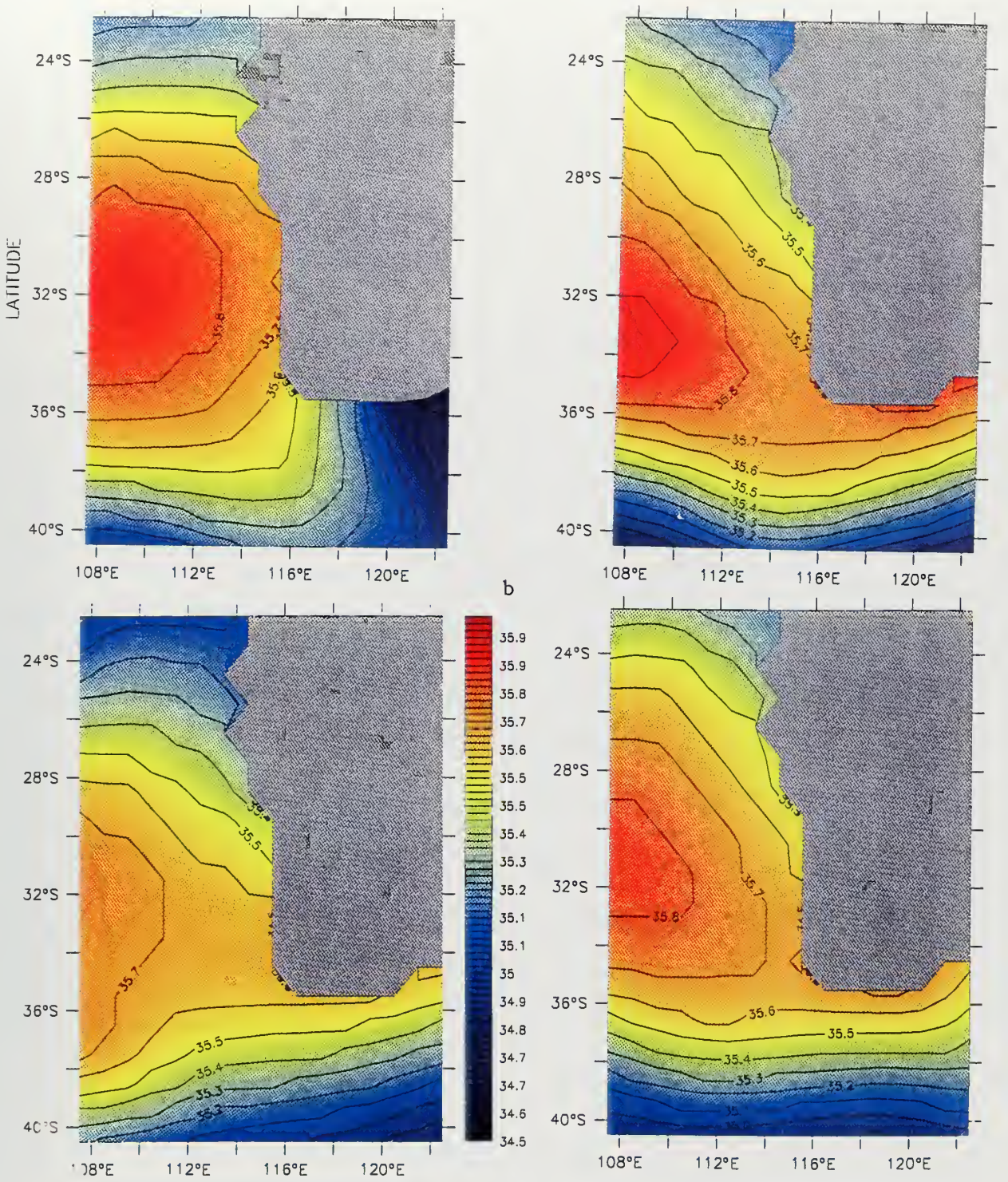
LATITUDE
24°S
28°S
32°S
36°S
40°S
108°E
112°E
116°E
120°E
b
35.9
35.9
35.8
35.7
35.6
35.5
35.5
35.4
35.3
35.2
35.1
35.1
35
34.9
34.8
34.7
34.7
34.6
34.5

Table 1. Values of Constants Used in the Model

Constant	Value	Definition
T_0	278.2°K	Constant Reference Temperature
S_0	34.7	Constant Reference Salinity
ρ_0	1.0276 gm cm^3	Density of Sea Water At T_0 and S_0
α	2.4×10^{-4} $(°K)^{-1}$	Thermal Expansion Coefficient
β	7.5×10^{-4}	Saline Expansion Coefficient
K	10	Number of Levels In Vertical
Δx	1.1×10^6 cm	Cross-Shore Grid Spacing
Δy	1.4×10^6 cm	Alongshore Grid Spacing
H	4.5×10^5 cm	Total Ocean Depth
Δt	800 s	Time Step
f_0	0.75×10^4 s^{-1}	Mean Coriolis Parameter
g	980 cm s^2	Acceleration of Gravity
A_M	2×10^{17} cm^4 s^{-1}	Biharmonic Momentum Diffusion Coefficient
A_H	2×10^{17} cm^4 s^{-1}	Biharmonic Heat Diffusion Coefficient
K_M	0.5 cm^2 s^{-1}	Vertical Eddy Viscosity
K_H	0.5 cm^2 s^{-1}	Vertical Eddy Conductivity

Table 2. The Design of The Experiments

Experiment #	Experiment
Response To Annual Forcing	
1	Variable Thermal Forcing with Constant Salinity Conditions
2	Variable Thermal and Salinity Forcing Conditions
Response To Seasonal Forcing	
3	Variable Thermal Forcing With Constant Salinity Conditions
4	Variable Thermal and Salinity Forcing Conditions

LIST OF REFERENCES

Andrews, J.C., "Eddy Structure and the West Australian Current." *Deep-Sea Res.*, 24, 1133-48, 1977.

Arakawa, A., and V.R. Lamb, "Computational Design of the Basic Dynamical Processes of the UCLA General Circulation Model." In, *Methods in Computational Physics*, J. Chang, ed., Academic Press, 17, 173-265, 1977.

Batteen, M. L., "Wind-forced Modeling Studies of Currents, Meanders, and Eddies in the California Current System." *J. Geophys. Res.*, Submitted, 1996.

Batteen, M. L., C. A. Collins, C. R. Gunderson, and C. S. Nelson, "The Effect of Salinity on Density in the California Current System." *J. Geophys. Res.,* 100, 8733-8749, 1995.

Batteen, M. L., C. L. Butler, and M.-J. Huang, "Modeling Studies of the Leeuwin Current off Western and Southern Australia." *J. Geophys Res.*, to be submitted, 1996.

Batteen, M.L., and Y.-J. Han, "On the Computational Noise of Finite-difference Schemes Used in Ocean Models." *Tellus*, 33, 387-396, 1981.

Batteen, M.L., M.J. Rutherford, "Modeling Studies of Eddies In the Leeuwin Current: The role of Thermal Forcing." *J. Phys. Oceanogr.*, 20, 1484-1520, 1990.

Batteen, M.L., M.J. Rutherford, and E.J. Bayler, "A Numerical Study of Wind and Thermal-forcing Effects on the Ocean Circulation off Western Australia." *J. Phys. Oceanogr.*, 22, 1406-1433, 1992.

Batteen, M.L., R.L. Haney, T.A. Tielking, and P.G. Renaud, "A Numerical Study of Wind Forcing of Eddies and Jets in the California Current System." *J. Mar. Res.*, 47, 493-523, 1989.

Boland, F. M., J. A. Church, A. M. G. Forbes, J. S. Godfrey, A. Huyer, R. L. Smith, and N. J. White, "Current-meter Data from the Leeuwin Current Interdisciplinary Experiment." *CSIRO Australia Marine Laboratory Report No. 198*, 1988.

Camerlengo, A.L. and J.J. O'Brien, "Open Boundary Conditions in Rotating Fluids. *J. Comput. Physics."* 35, 12-35, 1980.

Cresswell, G.R., and T.J. Golding, "Observations of a South-flowing Current in the Southeastern Indian Ocean." *Deep-Sea Res.*, 27A, 449-466, 1980.

Gentilli, J., "Thermal Anomalies in the Eastern Indian Ocean." *Nature (London) Physical Sciences,* 238, 93-95, 1972.

Godfrey, J.S., and K.R. Ridgway, "The Large-scale Environment of the Poleward-flowing Leeuwin Current, Western Australia: Longshore Steric Height Gradients, Wind Stresses and Geostrophic Flow." *J. Phys. Oceanogr.,* 15, 481-495, 1985.

Haney, R.L., "A Numerical Study of the Response of an Idealized Ocean to Large-scale Surface Heat and Momentum Flux." *J. Phys. Oceanogr.*, 4, 145-167, 1974.

Holland, W.R., "The Role of Mesoscale Eddies in the General Circulation of the Ocean-Numerical Experiments Using a Wind-driven Quasigeostrophic Model." *J. Phys. Oceanogr.*, 8, 363-392, 1978.

Holland, W.R., and M.L. Batteen, "The Parameterization of Subgrid Scale Heat Diffusion in Eddy-resolved Ocean Circulation Models." *J. Phys. Oceanogr.*, 16, 200-206, 1986.

Levitus, S., Climatological Atlas of the World Ocean. NOAA Professional Paper 13, 173 pp., US Department of Commerce: National Oceanic and Atmospheric Administration., 1982.

Levitus, S., R. Burgett, and T. P. Boyer, World Ocean Atlas 1994, Vol. 3: Salinity, *NOAA Atlas NESDI 3*, 99 pp., U. S. Dept. of Commerce, Washington, D. C., 1994.

Levitus, S. , and T. P. Boyer, World Ocean Atlas 1994, Vol. 4: Temperature, *NOAA Atlas NESDI 4*, 117 pp., U. S. Dept. of Commerce, Washington, D. C., 1994.

McCreary, J.P., Jr., S.R. Shetye and P.K. Kundu, "Thermohaline Forcing of Eastern Boundary Currents: with Application to the Circulation Off the West Coast of Australia." *J. Mar. Res.*, 44, 71-92, 1986.

Pickard, G. L., and W. J. Emery, *Descriptive Physical Oceanography*, 5th ed., 320 pp., Pergamon, New York, 1990.

Rochford, D.J., "Seasonal Variations in the Indian Ocean along 110 Degrees E. Part I: Hydrological Structure of the Upper 500 m." *Aust. J. Mar. Freshwater Res.*, 20, 1-50, 1969.

Rochford, D.J., "Seasonal Changes in the Distribution of Leeuwin Current Waters Off Southern Australia." *Aust. J. Mar. Freshwat. Res., 37*, 1-10, 1986.

Thompson, R.O.R.Y., "Observations of the Leeuwin Current off Western Australia." *J. Phys. Oceanogr.*, 14, 623-628, 1984.

Thompson, R.O.R.Y., "Continental-shelf-scale Model of the Leeuwin Current." *J. Mar. Res.*, 45, 813-827, 1987.

Weatherly, G.L., "A Study of the Bottom Boundary Layer of the Florida Current." *J. Phys. Oceanogr.*, 2, 54-72, 1972.

Weaver, A.J., and J.H. Middleton, "On the Dynamics of the Leeuwin Current." *J. Phys. Oceanogr.*, 19, 626-648, 1989.

INITIAL DISTRIBUTION LIST

		No. Copies
1.	Defense Technical Information Center 8725 John J. Kingman Rd., STE 0944 Ft. Belvoir, VA 22060-6218	2
2.	Dudley Knox Library Naval Postgraduate School 411 Dyer Rd. Monterey, California 93943-5101	2
3.	Chairman (Code OC/Bf) Department of Oceanography Naval Postgraduate School Monterey, California 93943-5122	1
4.	Chairman (Code MR/Hy) Department of Meteorology Naval Postgraduate School Monterey, California 93943-5114	1
5.	Dr. Mary L. Batteen, (Code OC/Bv) Department of Oceanography Naval Postgraduate School Monterey, CA 93943-5122	5
6.	Dr. Richard Lambert National Science Foundation 4201 Wilson Boulevard Arlington, VA. 22230	1
7.	Dr. T. Kinder Physical Oceanography Division Office of Naval Research 800 N. Quiney Street Arlington, VA. 22217	1

8.	Chinese Naval Hydrography and Oceanography Office P.O. Box 90186 TSO-YING Taiwan, R.O.C.	1
9.	Kao-Hsiung, Taiwan R. O. C. Chinese Naval Academic Library Tso-Ying, Kao-Hsiung Taiwan, R.O.C.	1
10.	LCDR Ming-Jer Huang P.O. Box 90186 TSO-YING Kao-Hsiung, Taiwan 81300 R. O. C.	2